J. Fluid Mech. (2007), *vol.* 587, *pp.* 271–301.
doi:10.1017/S0022112007007434 Printed in the United Kingdom

Transient growth in vortices with axial flow

C. J. HEATON AND N. PEAKE

Department of Applied Mathematics and Theoretical Physics, University of Cambridge, Wilberforce Road, Cambridge CB3 0WA, UK

(Received 23 October 2006 and in revised form 11 May 2007)

We investigate transient growth in high-Reynolds-number vortices with axial flow. Many cases of vortex instability are not fully explained by strong exponential instability modes, and transient growth could offer an alternative route to breakdown in such cases. Strong transient growth is found, in agreement with previous studies. We first discuss the problem by reference to ducted vortices which model aeroengine flow. The transient growth is inviscid in character, and in this paper we specifically interpret it as an effect of the inviscid continuous spectrum. The relevant inviscid theory explains new scalings which we find for the transient growth, which are generalizations of the quadratic scaling seen previously in two-dimensional flows and non-swirling pipe flows. We then turn to a second case, of interest for vortex breakdown, the Batchelor vortex, and present calculations of the transient growth. Large growth is possible, especially for the helical modes (with azimuthal wavenumber $|m| = 1$). The general trends are complicated by a number of issues, including a long-wavelength effect and a resonance effect, both of which were recently discovered for a vortex without axial flow and are found here to be present in the Batchelor vortex also. Overall, the results suggest that strong transient effects are present in the moderate- to high-swirl regime of practical interest (swirl number $q \gtrsim 2$). For axisymmetric ($m = 0$) and higher ($|m| > 1$) modes, however, transient effects are not found to be significant.

1. Introduction

At high Reynolds numbers vortices and swirling jets/wakes are known to be highly unstable and susceptible to breakdown. A variety of applications, from the trailing vortex behind a wing to tornadoes to swirling pipe flow, have provoked much research into understanding different breakdown phenomena. In this paper we investigate the effect of so-called transient growth mechanisms on high-Reynolds-number vortices with axial flow. We first present our ideas and identify mechanisms using a family of ducted flows, and then move on to the more complicated case of the Batchelor vortex (Batchelor 1964).

The phenomenon of transient growth results ultimately from the fact that the Navier–Stokes equations linearized about a non-trivial mean flow correspond to a non-normal operator. Linear systems governed by a normal operator have orthogonal eigenfunctions, and so knowledge of the spectrum is sufficient to determine whether a perturbation grows or decays. In a non-normal system, however, eigenfunctions are not orthogonal and as a result, even if the system is stable and all signals decay at large times, transient growth can occur at short times. The concept of transient growth has frequently been applied to hydrodynamic stability theory (Gustavsson 1991; Butler & Farrell 1992; Trefethen *et al.* 1993; Schmid & Henningson 1994). The transient phenomenon is quantified by considering an initial-value problem and asking what is

the maximum possible growth of, say, disturbance energy, the maximum being taken over all possible initial conditions. The initial condition corresponding to maximal growth is known as the optimal perturbation. The optimization problem posed can be solved numerically by a variety of methods, and in this paper we shall adopt the method of Corbett & Bottaro (2000), which will be described fully below. See Schmid & Henningson (2001) for a review of the ideas and of the results obtained in a variety of hydrodynamic stability problems. Substantial growth has been found to be possible even in stable shear flows and this has led to a great deal of interest, particularly with regard to the so-called 'bypass' route to transition of otherwise stable shear flows.

Much attention has been directed at the bypass transition of two-dimensional shear flows, and in contrast the first detailed investigations of transient growth in an isolated vortex have only recently appeared (Antkowiak & Brancher 2004; Pradeep & Hussain 2006). Batchelor's (1964) similarity solution for a trailing line vortex includes, importantly, axial flow. It gives a good fit of experimental data (e.g. Leibovich 1978, p. 231) and is the most commonly adopted model for theoretical study. A simpler two-dimensional vortex which differs only by neglecting the axial flow is known as the Lamb–Oseen vortex, and was the mean flow for the transient growth studies of Antkowiak & Brancher (2004) and Pradeep & Hussain (2006). Antkowiak & Brancher (2004) gave preliminary results for $m = 1$ (m the azimuthal wavenumber), finding large levels of transient growth. They found the growth to be peaked at a preferred axial wavenumber, and conjectured that this may result from a resonance phenomenon. Pradeep & Hussain (2006) performed similar calculations over a wider range of axial and azimuthal wavenumbers, and concluded that the $m = 1$ showed the most significant results. Pradeep & Hussain also gave detailed discussion of various physical and mathematical processes which they observed. Using a simplified model they concluded that a resonance phenomenon is present when $m = 1$, and gave predictions about the relevant optimal initial condition. One aim of the present paper is to present analogous results for the Batchelor vortex model, and the results of these two studies will form an important point of reference and comparison with many of our results.

As a prelude to the results for the Batchelor vortex, we will discuss in more general terms the transient problem for swirling flows. The mechanism for the growth seen in two-dimensional shear flows has been noted to be inviscid in nature (optimal initial conditions are streamwise streaks, which grow by the inviscid lift-up effect of Landahl 1980), and a similar observation has been made in the case of the Lamb–Oseen vortex (Antkowiak & Brancher 2004; Pradeep & Hussain 2006). We also find that this is the case, and indeed that for flows without conventional exponential instabilities the transient growth is really an effect of the inviscid continuous spectrum. Recent results by Heaton & Peake (2006) found that the contribution of the inviscid continuous spectrum is stronger and more complicated for swirling flows than for two-dimensional flows or pipe flows without swirl: instead of being neutrally stable, it can cause algebraic instability with disturbances growing as t^{σ}, where $\sigma > 0$. We explore the mechanism using an illustrative ducted flow which is simpler than the Batchelor vortex, and show that the transient growth in swirling flow is correspondingly stronger than for the non-swirling flow, with new scalings involving the exponent σ introduced. We find that the inviscid continuous spectrum theory gives an appealing interpretation of the results which captures the new scalings, as well as recovering the simpler scalings already known for non-swirling flows.

After introducing our ideas in the context of model ducted flows, our more detailed results are for the Batchelor vortex. Let us briefly recap the stability results for the

Batchelor vortex, a flow which has received considerable attention over the years. The Batchelor vortex has one free parameter controlling temporal stability, conventionally denoted q, which sets the relative strength of the rotational and axial velocities. The linear stability of the Batchelor vortex has been investigated numerically by Lessen, Singh & Paillet (1974), Duck & Foster (1980) and Mayer & Powell (1992) for inviscid flow, and at finite Reynolds number by Lessen & Paillet (1974), Khorrami (1991), Mayer & Powell (1992) and Fabre & Jacquin (2004). It is found that the vortex is susceptible to inviscid instabilities for all negative azimuthal wavenumbers. There also exist instabilities of a viscous nature, whose growth rates decay to zero in the limit $Re \to \infty$. The inviscid instabilities are the strongest of all the instabilities, but are restricted to relatively small values of q. Stewartson & Brown (1985) predicted that the inviscid vortex stabilizes for $q > 2.31$, a result that was confirmed by Heaton (2007), who also gave an expression for the rest of the inviscid neutral curve. However, while the inviscid instabilities are very strong for $q \lesssim 1.5$, they become dramatically weaker when q is increased beyond 1.5 (see Heaton 2007). Viscous instabilities persist to arbitrarily large q (Fabre & Jacquin 2004), but they are always weak, and so neither family of modal instabilities offers an immediate explanation for breakdown at swirl values of $q > 1.5$. In addition there is also the possibility of the algebraic instability of Heaton & Peake (2006), which is due to the continuous spectrum rather than discrete eigenvalues (i.e. *modes*). The Batchelor vortex is susceptible to algebraic instability as well, at all swirl levels, when $Re = \infty$. The strength of this effect, especially in the presence of a small but non-zero viscosity, is not known, and will form part of our investigation. In contrast to this complicated picture of instabilities for the Batchelor vortex, the Lamb–Oseen vortex (which corresponds to $q = \infty$) is always modally stable (Fabre, Sipp & Jacquin 2006), and also has a stable continuous spectrum (see (5.2), below).

Realistic values of q for which breakdown needs to be explained are usually around $q \gtrsim 2$ (Leibovich 1978), and so the modal instabilities alone can not account for what is observed. The algebraic instability, on the other hand, is formally absent at any finite Re, and so cannot provide the whole answer either. The possibility for short-time transient growth in this flow when for large times it is formally stable (or perhaps only weakly unstable, if a viscous mode is present) is therefore important to investigate. We shall see that transient growth can be large, and can still feel the effects of the various algebraic and exponential instabilities which are close by in parameter space. Should transient growth be sufficiently strong to induce nonlinear interactions then this might provide an alternative route to breakdown not reliant on strong long-time instabilities, and this possibility is the ultimate motivation for the present work. Two previous studies have considered transient growth in the Batchelor vortex (Schmid *et al.* 1993; Ben-Dov, Levinski & Cohen 2004), but they both considered a different regime: they looked at small q (specifically $q \leqslant 0.7$) to determine how transient effects might boost the exponential instabilities present at those swirl values. In contrast here we look at the large-q regime in which there are no strong instabilities, where transient effects might offer a different route to breakdown. Both Schmid *et al.* (1993) and Ben-Dov *et al.* (2004) demonstrated strong transient growth at the q values they considered, and we also find strong growth but, since we investigate a different mean-flow regime, detailed comparison is not appropriate.

The remainder of this paper is set out as follows. In § 2 the governing equations and boundary conditions are presented. In § 3 the transient growth problem is posed, and we discuss our numerical method for its solution. In § 4 mechanisms/scalings are investigated using a family of ducted vortices for illustration. In § 5 the detailed results for the Batchelor vortex are presented, and in § 6 we draw some conclusions.

2. Governing equations

We work in cylindrical coordinates (x, r, θ). The flow is incompressible, and we assume the following form for its mean profile

$$\boldsymbol{U}_0 = U(r)\boldsymbol{e}_x + W(r)\boldsymbol{e}_\theta. \tag{2.1}$$

Strictly speaking such mean flows only satisfy the Navier–Stokes equations when viscosity is neglected, but we shall make the usual assumption that this is a valid approximation, at least for mean profiles which are physically motivated from other arguments. In particular, the leading-order approximation of Batchelor's (1964) similarity solution for the trailing line vortex has the form (2.1); see (5.1).

The mean flow is subject to linear-small unsteady perturbations,

$$\left.\begin{aligned} \boldsymbol{u}_{\rm tot}(x, r, \theta, t) &= \boldsymbol{U}_0(r) + (u, v, w)\,\mathrm{e}^{\mathrm{i}m\theta + \mathrm{i}kx}, \\ p_{\rm tot}(x, r, \theta, t) &= p_0(r) + p\,\mathrm{e}^{\mathrm{i}m\theta + ikx}, \end{aligned}\right\} \tag{2.2}$$

where the azimuthal and axial wavenumbers $m \in \mathbb{Z}$ and $k \in \mathbb{R}$ are given constants. The complex amplitudes u, v, w and p are functions of (t, r). With prime denoting differentiation with respect to r, the linearized dimensional Navier–Stokes equations are

$$\frac{\partial u}{\partial t} + \left(\frac{Wm}{r} + Uk\right)\mathrm{i}u + vU' = -\mathrm{i}kp + \nu\left[\frac{(ru')'}{r} - \left(\frac{m^2}{r^2} + k^2\right)u\right], \tag{2.3}$$

$$\frac{\partial v}{\partial t} + \left(\frac{Wm}{r} + Uk\right)\mathrm{i}v - \frac{2Ww}{r} = -p' + \nu\left[\frac{(rv')'}{r} - \left(\frac{1+m^2}{r^2} + k^2\right)v - \frac{2\mathrm{i}mw}{r^2}\right], \tag{2.4}$$

$$\frac{\partial w}{\partial t} + \left(\frac{Wm}{r} + Uk\right)\mathrm{i}w + \frac{(Wr)'v}{r} = -\frac{\mathrm{i}mp}{r} + \nu\left[\frac{(rw')'}{r} - \left(\frac{1+m^2}{r^2} + k^2\right)w + \frac{2\mathrm{i}mv}{r^2}\right], \tag{2.5}$$

and the continuity equation is

$$\mathrm{i}ku + \frac{(rv)'}{r} + \frac{\mathrm{i}mw}{r} = 0. \tag{2.6}$$

The boundary conditions for (2.3)–(2.6) depend on the geometry, and are: no-slip (or impermeability if $\nu = 0$) at any duct walls, decay as $r \to \infty$ for unbounded flows, and for flows without a centre body kinematic conditions at $r = 0$ (Batchelor & Gill 1962; Khorrami, Malik & Ash 1989),

$$\left.\begin{aligned} m = 0: &\quad v = w = 0, \quad u, p \ \text{finite} \\ |m| = 1: &\quad u = v + \mathrm{i}mw = v' = p = 0 \\ |m| > 1: &\quad u = v = w = p = 0 \end{aligned}\right\} \ \text{at } r = 0. \tag{2.7}$$

For the calculations that follow we work with the state variable $\boldsymbol{v} \equiv (v, w)^t$, which satisfies the evolution equation

$$\frac{\partial}{\partial t}\mathscr{L}\boldsymbol{v} = \mathscr{M}\boldsymbol{v} + \nu\mathscr{N}\boldsymbol{v}. \tag{2.8}$$

Here $\mathscr{L}$ and $\mathscr{M}$ are second-order differential operators and $\mathscr{N}$ is a fourth-order differential operator; all three are obtained from elementary manipulations of (2.3)–(2.6) to eliminate p and u and are given in full in Appendix A. The original equations (2.3)–(2.6) are of mixed differential–algebraic type, since no time derivative appears in (2.6), whereas (2.8) is not mixed and so permits more straightforward computations. The boundary conditions for (2.8) are the same as for the full system.

Finally, the kinetic energy of a disturbance is

$$E(t) = \int_0^\infty \tfrac{1}{2}(|u|^2 + |v|^2 + |w|^2) r \,\mathrm{d}r = \tfrac{1}{2}\langle \boldsymbol{u}, \boldsymbol{u} \rangle, \tag{2.9}$$

which is the measure we shall use to test whether a disturbance is growing or decaying. The angle brackets in (2.9) denote the standard inner product,

$$\langle \boldsymbol{\alpha}, \boldsymbol{\beta} \rangle \equiv \int_0^\infty (\boldsymbol{\alpha}^*)^t \boldsymbol{\beta} r \,\mathrm{d}r, \tag{2.10}$$

where * denotes complex conjugate and ^{t} denotes matrix transpose.

3. The transient growth problem

3.1. *Definitions*

Using the kinetic energy norm (2.9), the energy amplification at a given time and for a given initial condition is $E(t)/E(0)$. We wish to find how large this quantity can become by varying the initial conditions, $\boldsymbol{u}(t=0)$. The maximum energy amplification, over all possible initial conditions, at a given time is called the *gain*, $G(t)$. The gain curve $G(t)$ provides an envelope for all possible curves of energy amplification as a function of time. At finite Re flows which are stable, so that all disturbances decay at long times via viscous diffusion, have a maximum gain

$$G_{\max} = \max_t G(t), \tag{3.1}$$

where $G_{\max} = G_{\max}(Re, \boldsymbol{U}_0, m, k)$ depends on the Reynolds number, the mean flow and the wavenumbers m, k. The time at which $G(t)$ reaches $G_{\max}$ is $t_{\max}$, and the initial disturbance whose energy amplification attains the gain $G_{\max}$ is known as the optimal perturbation. A more detailed description of these concepts can be found in Schmid & Henningson (2001).

In most cases $G_{\max}$ will be our primary measure of how large transient effects may be; however, it is also important to note the shape of the rest of the gain curve. In some circumstances we will find that large optimal gains, while theoretically possible, would require such long times to evolve as to be physically meaningless. It is also important to check that the spatial structure of the optimal initial condition for transient growth is physically feasible (in some sense). The question of how a shear flow responds to continuous stochastic forcing (as a model of weak turbulence or other noise in an experiment) was addressed by Farrell & Ioannou (1993), who found that the process was closely related to the standard transient growth mechanism. While the feasibility of the optimal initial condition must play an important role in the applicability of any transient growth result, we will limit ourselves in this paper to the idea that initial conditions localized far away from the vortex core are unlikely to be important. One intuitively expects that such conditions are unlikely to be excited by random noise, but more concretely the assumption made in this paper that the mean flow is an isolated vortex must fail far from the vortex core. Hence some care is required, and both the spatial structure of the optimal initial condition and the time scale for the transient growth should be borne in mind when interpreting the raw results for $G_{\max}$.

To find the gain $G(t)$ we have followed the approach of Corbett & Bottaro (2000). Details of how the optimization problem is posed, and numerically solved, are given in the following subsections.

3.2. *Theory*

Using (2.6) we may readily define an operator $\mathscr{A}$ (given in full in Appendix A) such that $\boldsymbol{u} = \mathscr{A}\boldsymbol{v}$ to recover the full velocity vector from the state variable $\boldsymbol{v}$. Let us also define formally the propagation operator $\mathscr{P}(t) \equiv \exp\left(\mathscr{L}^{-1}(\mathscr{M} + \nu\mathscr{N})t\right)$. This definition just corresponds formally to solving (2.8), so that $\boldsymbol{v}(t) = \mathscr{P}(t)\boldsymbol{v}(0)$. The energy amplification at time t is then given by

$$\frac{E(t)}{E(0)} = \frac{\langle \mathscr{A}\mathscr{P}(t)\boldsymbol{v}(0), \mathscr{A}\mathscr{P}(t)\boldsymbol{v}(0)\rangle}{\langle \mathscr{A}\boldsymbol{v}(0), \mathscr{A}\boldsymbol{v}(0)\rangle} = \frac{\langle \boldsymbol{v}(0), \mathscr{P}(t)^{\dagger}\mathscr{A}^{\dagger}\mathscr{A}\mathscr{P}(t)\boldsymbol{v}(0)\rangle}{\langle \boldsymbol{v}(0), \mathscr{A}^{\dagger}\mathscr{A}\boldsymbol{v}(0)\rangle}, \tag{3.2}$$

where † represents the adjoint with respect to the inner product (2.10). The maximum energy amplification, the gain $G(t)$, is found by maximizing the quotient (3.2) and is hence the largest eigenvalue of the system

$$\left(\mathscr{A}^{\dagger}\mathscr{A}\right)^{-1}\mathscr{P}(t)^{\dagger}\mathscr{A}^{\dagger}\mathscr{A}\mathscr{P}(t)\boldsymbol{v}(0) = G(t)\boldsymbol{v}(0). \tag{3.3}$$

The eigenvalue problem (3.3) must be solved, and so let us consider more carefully the meaning of the operators it contains. Of course, in general it is not practical to obtain the operator $\mathscr{P}(t)$ by direct exponentiation as we initially defined it. Instead we will discretize the associated evolution equation (2.8) and solve it numerically, as is described in § 3.3 below, to obtain the action of $\mathscr{P}(t)$. In order to obtain the effect of $\mathscr{P}^{\dagger}(t)$ we will numerically solve an adjoint equation. We choose to define our adjoint equation by taking (2.8) and simply replacing each operator appearing in (2.8) by its adjoint, so

$$\frac{\partial}{\partial t}\mathscr{L}^{\dagger}\boldsymbol{w} = \mathscr{M}^{\dagger}\boldsymbol{w} + \nu\mathscr{N}^{\dagger}\boldsymbol{w}. \tag{3.4}$$

Using the operator identity $\exp(\mathscr{B}) \equiv \mathscr{C}^{-1}\exp(\mathscr{C}\mathscr{B}\mathscr{C}^{-1})\mathscr{C}$, it is quickly shown that the propagation operator for the adjoint equation (3.4), $\mathscr{Q}(t)$ say, is given by

$$\mathscr{P}^{\dagger}(t) = \mathscr{L}^{\dagger}\mathscr{Q}(t)(\mathscr{L}^{\dagger})^{-1}. \tag{3.5}$$

Solution of the adjoint equation therefore can be used to obtain the action of $\mathscr{P}^{\dagger}(t)$. We can now numerically approximate all the required operators in (3.3) by solving discretized equations: the operators $\mathscr{A}$ and $\mathscr{L}$ can be obtained directly, and $\mathscr{P}(t)$ and $\mathscr{P}^{\dagger}(t)$ can be obtained by numerical solution of (2.8) and the related adjoint equation. A further simplification is made possible by the following result, which can easily be shown from first principles using Appendix A, although the detailed algebra is not included:

$$(\mathscr{L}^{\dagger})^{-1}(\mathscr{A}^{\dagger}\mathscr{A}) = -\frac{1}{k}\begin{pmatrix} 0 & \mathscr{I} \\ \mathrm{i}\mathscr{I} & 0 \end{pmatrix} \tag{3.6}$$

where $\mathscr{I}$ is the identity operator. Equations (3.5)–(3.6) together imply that (3.3) is equivalent to

$$\begin{pmatrix} 0 & -\mathrm{i}\mathscr{I} \\ \mathscr{I} & 0 \end{pmatrix}\mathscr{Q}(t)\begin{pmatrix} 0 & \mathscr{I} \\ \mathrm{i}\mathscr{I} & 0 \end{pmatrix}\mathscr{P}(t)\boldsymbol{v}(0) = G(t)\boldsymbol{v}(0), \tag{3.7}$$

and hence only $\mathscr{P}(t)$ and $\mathscr{Q}(t)$ need to be computed. Further, the transfer matrix to the left of $\mathscr{P}(t)$ in (3.7) allows us to identify the boundary conditions appropriate to the adjoint problem: the first component of the adjoint variable has the same boundary conditions as w, while the second component of the adjoint variable acts as $\mathrm{i} \times v$.

3.3. *Numerical method*

The numerical solution of the eigenvalue problem (3.7) requires the solution of (2.8) and its related adjoint equation. We discretize the radial coordinate using a standard Chebyshev pseudospectral method (Boyd 2001) to obtain matrix approximations to the operators $\mathscr{L}$, $\mathscr{M}$ and $\mathscr{N}$. For open vortices the semi-infinite radial domain $r \in [0, \infty]$ is mapped to the interval $\xi \in [-1, 1]$ via the transformation $\xi = (r - L)/(r + L)$. The parameter L is free to be chosen and does not affect the end results; in what follows we used $L = 1.5$. Note that this means we do not need to artificially truncate the computational domain at some large radius. For ducted vortices a linear transformation is taken from r to ξ. For most of the presented results we used $N = 100$ or $N = 150$ collocation points and Chebyshev polynomials. Temporal discretization was performed using the first-order backward Euler method. This time-stepping method is unconditionally stable, the value of the time step being adjusted to ensure satisfactory convergence; in all cases a convergence tolerance of 1% or less was used. For the viscous calculations shown in figure 7 we found it to be efficient to choose initially a coarse time step in order to give an estimate for $t_{\max}$, and then to refine the time step until an accurate optimal was obtained. For inviscid calculations it was found that the time marching could be accurately replaced with direct matrix exponentiation of the spatially discretized problem, which was found to be quicker for these cases. With these numerical approximations to the operators $\mathscr{P}(t)$ and $\mathscr{Q}(t)$, the eigenvalue problem (3.7) was solved for the largest eigenvalue using the power method, convergence usually requiring 5–10 iterations. The power method is initiated with an input for $\boldsymbol{v}(0)$ on the first iteration. The gain which is converged upon by the power method does not depend on the starting condition (unless an exceptionally unlucky choice is made: e.g. a vector which belongs to an invariant subspace of the operator on the left-hand side of 3.7). That the gain $G(t)$ was insensitive to the starting condition for the power method iterations was explicitly checked for a representative subset of the calculations. All calculations were performed in MATLAB$^{\text{TM}}$ or Octave$^{\text{TM}}$ on standard desktop computers.

We numerically validated our code in two ways. First, the accuracy of the spatial discretization was tested by assuming exponential time dependence and then solving the associated eigenvalue problem for the complex frequencies. For the Batchelor vortex this was compared with published results for the eigenfrequencies (Mayer & Powell 1992), and also with the results of a separate code developed independently and described by Heaton (2007), which uses a completely different 'shooting' method. Second, as a verification of the time-stepping procedure and the power method for the optimal gain $G(t)$, we set $q = \infty$ in the Batchelor vortex to recover the two-dimensional Lamb–Oseen vortex. The optimal growth $G_{\max}$ for this vortex has been reported by Antkowiak & Brancher (2004) and Pradeep & Hussain (2006), and our results for $q = \infty$ are in agreement with theirs.

4. Ducted vortices

4.1. *Preliminaries*

In this section we shall adopt a simple family of ducted swirling flows to motivate a discussion of the transient effects in general vortices. The mean flow we consider is a commonly used model for the swirling flow downstream of the fan in aeroengine ducts (Atassi *et al.* 2004; Cooper & Peake 2005). The swirl is a combination of solid-body rotation and a free vortex, and the axial flow is determined by the assumption

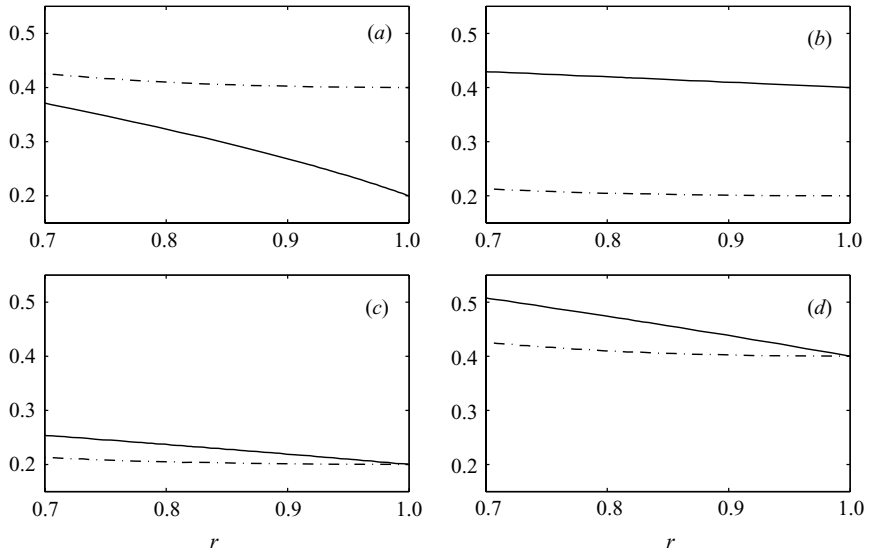

FIGURE 1. Plots of the mean-flow profiles (4.1)–(4.2) with (Ω, Γ, U_0) given by (*a*) (0.2, 0.2, 0.2), (*b*) (0.1, 0.1, 0.4), (*c*) (0.1, 0.1, 0.2) and (*d*) (0.2, 0.2, 0.4). In each case $U(r)$ is the solid line, and $W(r)$ the dash-dotted line.

of uniform stagnation enthalpy. We use the duct outer radius and a representative velocity value to non-dimensionalize the problem in this section. The mean flow is given by

$$\{U(r)\}^2 = U_0^2 - 2\left\{\Omega^2(r^2-1) + 2\Omega\Gamma\log(r)\right\}, \tag{4.1}$$

$$W(r) = \Omega r + \Gamma/r, \tag{4.2}$$

where $h \leqslant r \leqslant 1$ as the flow is confined in an annular duct. The mean radial pressure gradient is determined by the radial force balance, while the flow is assumed incompressible so that the mean density is uniform. In fact, compressibility of the flow does not affect the values of $\sigma(r)$ in what follows, and therefore the $t \to \infty$ behaviour we are about to describe is unaffected, although of course the transient growth at $O(1)$ times is affected by compressibility. In the calculations which follow in § 4.2 we always have $\Omega, \Gamma > 0$ (see (4.8)), and hence the mean flows (4.1)–(4.2) have axial flow which decreases monotonically with radius. Figure 1 shows the mean flow profiles for four of the cases we later use in our computations.

We anticipate that the mechanism for transient growth will be inviscid in nature, and so let us apply the results of Heaton & Peake (2006) to the flow (4.1)–(4.2). The inviscid continuous spectrum is given by the set of frequencies

$$C_\omega = \{\omega_c(r) \ : \ h \leqslant r \leqslant 1\}, \tag{4.3}$$

where

$$\omega_c(r) = U(r)k + mW(r)/r. \tag{4.4}$$

Each frequency in the continuous spectrum contributes to the solution of an initial value problem in such a way that it is approximately convected by the local mean flow, and with an algebraic amplitude. Specifically, $|\boldsymbol{u}| \sim t^{\sigma(r)}$ as $t \to \infty$ where

$$\sigma(r) = \mathrm{Re}\left(-\tfrac{1}{2} + \sqrt{\tfrac{1}{4} - A(r)}\right), \tag{4.5}$$

$$A(r) = \frac{2Wk(k(Wr)' - mU')}{r^2(m(W/r)' + kU')^2}. \tag{4.6}$$

The overall contribution of the continuous spectrum to the radially integrated energy (2.9) is $E(t) \sim t^{2\sigma_{\max}}$, where

$$\sigma_{\max} = \max_r \sigma(r). \tag{4.7}$$

The algebraic behaviour depends on the mean-flow parameters U_0, Ω and Γ, and also the wavenumbers m and k in a complicated manner, leading to many different cases. In particular, it may be that $\sigma_{\max} = \infty$, in which cases the continuous spectrum contribution does not have a simple algebraic scaling with t. Also, when $\sigma_{\max} = \infty$ the flow can support exponential instabilities of the type described by Heaton & Peake (2006) (although it is possible that $\sigma_{\max} = \infty$ without exponential instability, e.g. in the white regions below the lines in figure 5). We will concentrate in this section on cases with $\sigma_{\max}$ finite, as our interest is restricted to cases without exponential instabilities (where transient effects may provide a *new* mechanism for instability), and also because the simpler scalings will allow a clearer investigation of the transient effects.

4.2. *Transient growth*

We perform transient growth calculations on the ducted flow (4.1)–(4.2) with the hub radius $h = 0.7$ and for a variety of values of the other parameters:

$$\left.\begin{array}{lll} \Omega \in \{0.1,\ 0.2,\ 0.3\}, & \Gamma \in \{0.1,\ 0.2,\ 0.3\}, & U_0 \in \{0.2,\ 0.3,\ 0.4\}, \\ k \in \{1,\ 2,\ 3\}, & -5 \leqslant m \leqslant 5. & \end{array}\right\} \tag{4.8}$$

We found, as anticipated from the results for two-dimensional shear flows (Schmid & Henningson 2001) and also the Lamb–Oseen vortex (Antkowiak & Brancher 2004; Pradeep & Hussain 2006), that large transient effects are possible. As for those other flows, the mechanism for transient growth is inviscid, and viscosity is seen to have a simple damping effect. Further, we find that for flows without modal instabilities, the strong inviscid growth is specifically a continuous spectrum effect. To demonstrate this statement we will present some strictly inviscid results for the gain in this section.

Consider an inviscid modally stable flow, for which we have already argued the energy $E(t) \sim t^{2\sigma_{\max}}$ for large t from the continuous spectrum, plus stable exponential contributions from the discrete modes. However, the gain $G(t)$ does not share the same scaling, because for each different time t a new optimization is performed and the initial conditions therefore change. Appendix B shows that in fact we should expect

$$G(t) \sim t^{2+2\sigma_{\max}} \quad \text{for} \quad t \gg 1, \tag{4.9}$$

essentially because allowing the solution to evolve for longer times before observing the energy means a more effective initial condition can be chosen to optimize the gain. The behaviour (4.9) was observed in our calculations, and figure 2 shows six illustrative examples taken from the cases (4.8). The mean flows for the cases shown in figure 2 are plotted in figure 1. Figure 2 shows a good agreement between the expected scaling (4.9), visible in the gradients of the straight-line segments, and the transient growth calculations shown by the dots. It is expected that the scaling will be realized at later times in cases with larger values of $\sigma_{\max}$ (see Heaton & Peake 2006), which makes accurate calculation more difficult in these cases. Correspondingly, the best agreement is seen for the cases with smaller $\sigma_{\max}$. One other flow, namely compressible rigid-body swirl with uniform axial flow, should be mentioned in support

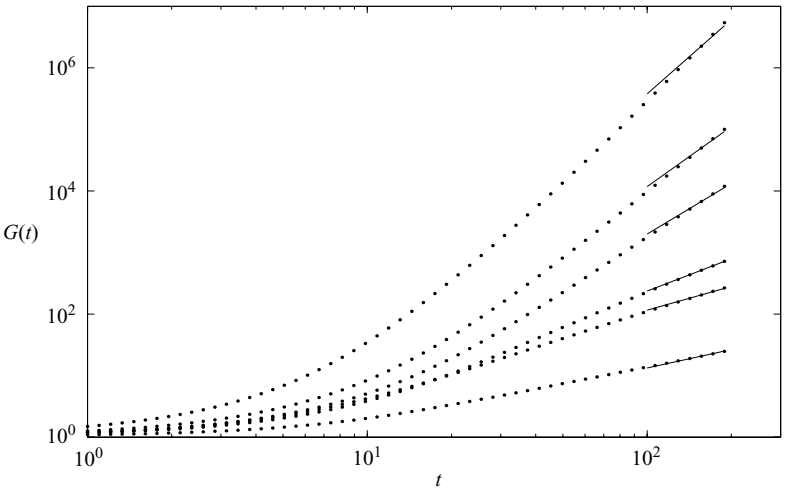

FIGURE 2. Some example inviscid gains for flows in the annular duct $0.7 \leqslant r \leqslant 1$. For the six cases shown, from bottom to top, $2 + 2\sigma_{\max} = 1.00, 1.27, 1.74, 2.73, 3.23$ and 4.00. In each case a straight-line segment of gradient $2 + 2\sigma_{\max}$ is shown for comparison. The parameters $(\Omega, \Gamma, U_0, k, m)$ take the values $(0.2, 0.2, 0.2, 1, 0)$, $(0.1, 0.1, 0.4, 3, 5)$, $(0.1, 0.1, 0.2, 1, 4)$, $(0.1, 0.1, 0.2, 1, -5)$, $(0.2, 0.2, 0.4, 1, -3)$ and $(0.2, 0.2, 0.2, 1, -5)$, respectively.

of our description of the transient gain as a continuous spectrum effect. This is a non-trivial flow which has no continuous spectrum but which does exhibit transient growth (NB the compressibility is important: an incompressible flow with this profile is trivial and does not exhibit transient growth). Cooper & Peake (2006) computed the transients for this flow but they found very little growth ($G(t) < 6$ in the cases they presented), and that the inviscid gain did not increase without bound, which is consistent with our arguments in Appendix B.

In addition to describing the large-t scaling for a particular case, the scaling (4.9) also gives an indication of which modally stable flows can be expected to have the greatest transient growth. Figure 3(a) shows the gain at $t = 50$ for all the cases given by (4.8) for which $2 + 2\sigma_{\max} < 20$. The general trend is that the gain is positively correlated with $\sigma_{\max}$ as expected. Figure 3(a) summarizes 765 different cases, and a large amount of scatter is seen on the plot. This is because, while (4.9) gives the exponent of the large-t gain, the prefactor will be determined by a variety of other effects on a case-by-case basis. For each value of $\sigma_{\max}$ in figure 3(a) the gain varies over at least two decades, but nevertheless the data collapse well onto the predicted line in figure 3(b). The cases with larger $\sigma_{\max}$ are expected to take longer times to fully realize (4.9), which is why the rightmost data points in figure 3(b) are not yet close to the dashed line showing the asymptotic prediction.

To summarize, for inviscid swirling flows large transient growth is found to be possible. If the flow is modally unstable then the transient gain will reflect this and grow exponentially, but otherwise (as seen in our results) the continuous spectrum will generate large gains at algebraic rates. The important remaining question to address is that of the action of viscosity on the inviscid arguments we have presented. The action of viscosity is most simply characterized by imagining that the inviscid growth mechanism is halted by dissipation, which takes over at a time determined by the value of Re. In general, linear disturbances to shear flows are dissipated by the shear-diffusion mechanism (see Bernoff & Lingevitch 1994 for a description

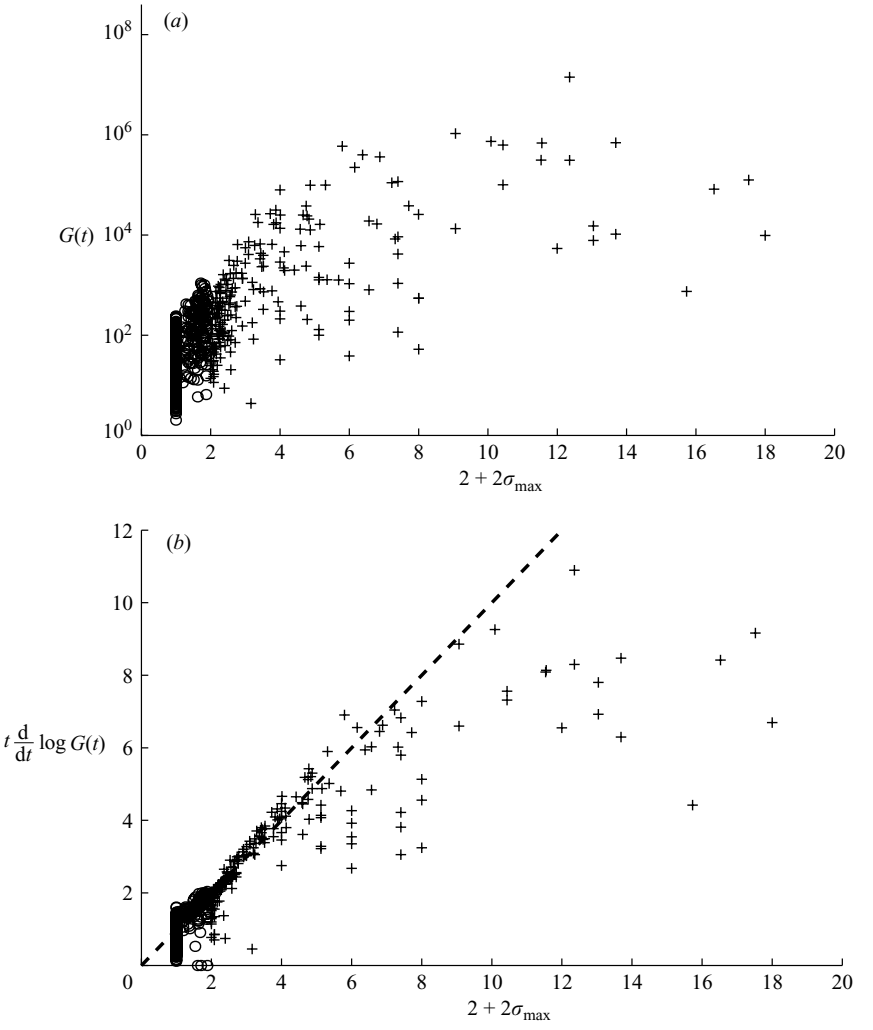

FIGURE 3. (*a*) The inviscid gain and (*b*) its logarithmic derivative at $t = 50$ for all the flows given by (4.8) in the annular duct $0.7 \leqslant r \leqslant 1$. Cases for which $\sigma_{\max} > 0$ are plotted with a + symbol, cases for which $\sigma_{\max} < 0$ with a ∘ symbol. The dashed line in (*b*) has gradient 1 and passes through the origin.

of the physical mechanism), which acts on a time scale $O(Re^{1/3})$. The $Re^{1/3}$ time scale was first identified by Thomson (1887), while Chapman (2002) gives a recent mathematical description in the context of transient growth and bypass transition. There are however exceptions to the rule, the most important being as follows.

(*a*) In two-dimensional shear flows and non-swirling pipe flows, streamwise independent disturbances decay on the longer $O(Re)$ time scale. See Gustavsson (1991), Schmid & Henningson (2001) and Chapman (2002) for details.

(*b*) In vortices without axial flow axisymmetric disturbances decay on the longer $O(Re)$ time scale. See Bernoff & Lingevitch (1994).

For the vortices with axial flow we consider here, the same exceptional behaviour only occurs if both $m = k = 0$, in which case the arguments used by Chapman (2002) (for instance) follow in exactly the same way. The exceptional case (*a*) above is

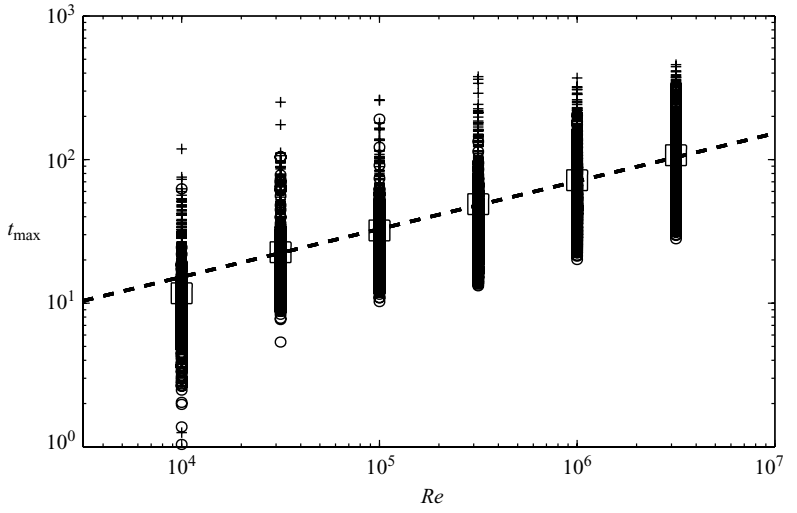

FIGURE 4. Values of $t_{\max}$ for the cases given by (4.8) at varying Re. The mean value for each Re is shown by □, and the dashed line has gradient 1/3.

important to bypass transition scenarios (see § 4.3); however, that special behaviour does not translate to the three-dimensional flows we consider here and $m = k = 0$ does not have any significance. This is because, on setting $m = k = 0$ and $Re = \infty$, the inviscid problem degenerates so that the operator becomes normal, and no transient growth whatsoever is possible.

Taking the time scale dictated by shear diffusion (ignoring the special cases), we have that $t_{\max} \sim Re^{1/3}$. This scaling, combined with (4.9), would imply that $G_{\max} \sim Re^{(2+2\sigma_{\max})/3}$. Now, when $Re < \infty$ the inviscid continuous spectrum is formally absent, and is replaced instead by a large number of stable discrete modes with weak decay rates. Since the arguments of Appendix B involve the continuous spectrum, they only apply to the purely inviscid case. However, thinking of the initial value problem written in the form (2.8), all the properties of the inviscid problem should still hold for sufficiently early times, implying that the result (4.9) will be robust to the introduction of viscosity until the viscous time scale is reached. At this and later times, the inviscid growth (4.9) will cease and viscous decay will set in. Numerically we confirmed in figures 2 and 3(*b*) that (4.9) holds for the inviscid growth stage, but we were not able to directly confirm the scaling of $G_{\max}$ on Re. This was because accurate computations were only possible over a limited range of Re, for which $t_{\max}$ was too small for (4.9) to be fully realized. However, we found that the alternative numerical method employed by Schmid *et al.* (1993) (fully detailed in that paper) was accurate over a slightly larger range of Re. We used this alternative method to produce figure 4, which confirms the expected scaling $t_{\max} \sim Re^{1/3}$. Therefore we would conjecture that the scaling

$$G_{\max} \sim Re^{(2+2\sigma_{\max})/3} \tag{4.10}$$

will hold as $Re \to \infty$ for these flows, although a direct confirmation was not possible. To summarize: the gain curve first grows according to (4.9), the Reynolds number dictates the magnitude of $t_{\max}$, and these combined give the size of the optimal gain.

The relation of the scalings presented to the results previously published on transient growth in non-swirling flows will be discussed in the next subsection. First, however,

we should note that swirling flows can possess viscous modes, for which viscosity has a weakly *destabilizing* action. This will be discussed more fully in the context of the Batchelor vortex below, because that flow is known to possess such modes (Khorrami 1991; Fabre & Jacquin 2004). For now it suffices to state that the continuous spectrum mechanism for transient growth dominates such modes at early times. Viscous instabilities, if present, would not affect the transient gain until late times, when their weak exponential growth catches up to the inviscid effect described here. For example, the strongest family of viscous modes in the Batchelor vortex has exponential growth rates $O(Re^{-1/3})$ (see Le Dizès & Fabre 2006), so at $t = O(Re^{1/3})$ these modes have only grown by an $O(1)$ amount, which is much less than the gain (4.10) possible by inviscid processes. Whether viscous modes are present or not, the inviscid mechanism governs the gain curve (see the dashed line in figure 6) until later times.

4.3. *Relation to transient growth in non-swirling flow*

We wish to compare the scaling (4.9) and the associated results in figures 2 and 3 with the results found previously in other shear flows. We are thinking primarily of parallel two-dimensional shear flows $\boldsymbol{U}_0 = U(y)\boldsymbol{e}_x$, but also non-swirling circular flows such as Hagen–Poiseuille flow. Herein we use the term 'non-swirling flows' to refer collectively to both these types of flow.

Considering the parallel two-dimensional shear flow, let the streamwise and spanwise wavenumbers be α and β, respectively. The continuous spectrum is given by

$$C_\omega = \{\alpha U(y)\}, \tag{4.11}$$

where y ranges over all the locations in the flow. The continuous spectrum again contributes algebraically in the inviscid case, but now we have $|\boldsymbol{u}| \sim t^\sigma$ with

$$\left.\begin{array}{ll} \sigma = 0 & \text{for } \alpha \neq 0, \\ \sigma = 1 & \text{for } \alpha = 0, \end{array}\right\} \tag{4.12}$$

for all y; see Landahl (1980) for details. The inviscid linear growth of the streamwise independent disturbances is known as the lift-up effect. If $\alpha \neq 0$ then by Appendix B the inviscid gain will grow as $G(t) \sim t^2$. For $\alpha = 0$ the continuous spectrum C_ω degenerates to a single point and the mechanism of Appendix B no longer provides an extra t^2 factor, but since $\sigma = 1$ in this case we again recover $G(t) \sim t^2$. Exactly analogous results follow for the non-swirling circular pipe flows as well. Non-swirling flows therefore correspond to $2 + 2\sigma_{\max} = 2$, and lie on the boundary between the $\circ$ and $+$ symbols in figure 3. Swirling flows, in contrast, have a continuous spectrum with a wider variety of possible responses, and figure 3 shows that swirling flows can have either weaker or stronger transient gains as a result.

A result common amongst the many studies of non-swirling flows is that the maximum transient growth occurs at $\alpha = 0$ and scales as $G_{\max} \sim Re^2$, with $t_{\max} \sim Re$. This result is found by Gustavsson (1991), Butler & Farrell (1992), Trefethen *et al.* (1993), Schmid & Henningson (1994), Hanifi & Henningson (1998) and others. These scalings can be supported by a rescaling of the linearized equations setting $\alpha = 0$, first performed by Gustavsson (1991) (see also the review of Schmid & Henningson 2001). The same scalings can also be recovered using an interpretation based on the continuous spectrum. As we have seen, the rate at which the gain curve increases with time is dictated by the inviscid problem, and so is quadratic in time for all α as argued above. The $\alpha = 0$ case is then selected for maximum growth at fixed Re

because of the longer $O(Re)$ time scale for viscous damping discussed in § 4.2.† We suggest this alternative interpretation, of inviscid continuous spectrum growth with $G(t) \sim t^2$ which is halted at $t_{\max} \sim Re$ by viscous damping, as a general explanation.

Note that the inviscid stage of the growth for which (4.9) applies is $1 \ll t \ll t_{\text{visc}}$, where the viscous time scale is usually $t_{\text{visc}} = Re^{1/3}$, but for the case of $\alpha = 0$ in non-swirling flow $t_{\text{visc}} = Re$. An additional check on our arguments is to set $1 \ll t \ll Re$ in the model problem for $\alpha = 0$ disturbances given in the Appendix of Schmid & Henningson (1994). For these times Schmid & Henningson's model problem can be seen to have $G(t) \sim t^2$. Hence the quadratic shape of the gain curve before the maximum, as well as the scaling for its maximum itself, agrees with their arguments.

We believe that the mechanism for the transient growth in inviscid shear flows can be well described as a continuous spectrum effect, with the ability to range over a continuum of responses to optimize the gain an important concept. Decomposing the viscous problem into an inviscid growth stage and a viscous cutoff allows the tractable theory of the inviscid problem to be applied, and in this way the continuous spectrum argument recovers the quadratic scaling of $G_{\max}$ for non-swirling flows. This interpretation also generalizes naturally to cover the wider range of scalings which become possible for swirling flow, as seen in § 4.2. The differences for swirling flows are just that the exponent $\sigma_{\max}$ can take a wide range of values, and that the time scale for viscous damping reverts to its (usual) $Re^{1/3}$ scale. Now, since the $Re^{1/3}$ shear-diffusion time scale applies to oblique ($\alpha \neq 0$) waves in non-swirling flow, the continuous spectrum arguments should directly recover the published results for these waves too. Chapman (2002) showed that for oblique modes $G_{\max}$ scales as $Re^{2/3}$ in plane Couette and plane Poiseuille flow (see p. 56 and figures 21–25 of Chapman 2002, and note that the 'maximum norm' discussed there is the square root of the 'gain' in the present paper). The $Re^{2/3}$ behaviour is correctly recovered by our arguments on setting $2 + 2\sigma_{\max} = 2$ in equation (4.10).

We believe that the general details of the inviscid transient problem have not previously been discussed in the manner of Appendix B and the result (4.9) before, most likely because the results for non-swirling flows can be explained adequately by the rescaling of the viscous equations. Analysing the finite-Re gain curve in terms of an inviscid growth stage which is followed by viscous decay has been done previously (e.g. Trefethen *et al.* 1993; Hanifi & Henningson 1998; Pradeep & Hussain 2006), but without separate detailed analysis of the inviscid gain curve. Nevertheless, the result that the inviscid gain $G(t) \sim t^2$ for non-swirling flows is in fact visible in figure 7 of Trefethen *et al.* (1993) for plane Couette flow, and figures 1 and 2 of Hanifi & Henningson (1998) for a compressible boundary layer flow. The attraction of the interpretation suggested in this section is that the more complicated scalings of swirling flows fit naturally into the framework. The interpretation we suggest should complement the many alternative descriptions of transient effects. These include discussing physical mechanisms (Schmid & Henningson 2001; Pradeep & Hussain 2006), arguing from special-case instabilities (e.g. the lift-up effect, or § 3.2.1 of Pradeep & Hussain 2006), or setting $\alpha = 0$ and rescaling the Orr–Sommerfeld equation (Gustavsson 1991; Schmid & Henningson 2001).

† That the $\alpha = 0$ modes are optimal because of their slower viscous damping has been observed before (Schmid & Henningson 1994; Chapman 2002; and others), but we wish to show that all the findings can alternatively be derived using continuous spectrum arguments. Note also that the lift-up effect *per se* is not the selection criterion, as the inviscid transient gain grows at the same (quadratic) rate when $\alpha \neq 0$.

5. The Batchelor vortex

5.1. *Preliminaries*

For the Batchelor vortex we will scale lengths and velocities with the vortex core radius and swirl velocity, respectively, so that our mean flow in this section becomes

$$\left.\begin{aligned} U(r) &= a + q^{-1}\,\mathrm{e}^{-r^2}, \\ W(r) &= (1-\mathrm{e}^{-r^2})/r. \end{aligned}\right\} \tag{5.1}$$

We may set the advection parameter $a=0$ from now on, as it has no effect on temporal stability (either modal or transient), corresponding to a Galilean shift. Scaling our velocities on a characteristic value of the swirl causes (5.1) to appear slightly different to the usual representation of the Batchelor vortex (see, for example, equation (1) of Mayer & Powell 1992), but the two are equivalent. The scaling (5.1) will aid comparison with the Lamb–Oseen vortex (which is obtained by setting $q=\infty$), and also clarify the effect of increasing the axial flow in the vortex (corresponding to decreasing q). Following Pradeep & Hussain (2006) we shall use a vortex Reynolds number defined by the circulation (at infinity) divided by viscosity. For vortex breakdown we are concerned with moderate to high Reynolds numbers, say $Re \geqslant 1000$, and the swirl regime $q \gtrsim 2$ (Leibovich 1978). Also, the low azimuthal orders are the most important (Leibovich 1978), with experiments observing breakdown to occur either at $m=0$ (bubble type) or $m=\pm 1$ (spiral type).

The Lamb–Oseen vortex studied by Antkowiak & Brancher (2004) and Pradeep & Hussain (2006), i.e. (5.1) with $q=\infty$ and therefore no axial flow, is two-dimensional and is always linearly stable (Fabre *et al.* 2006). The Batchelor vortex, with $q<\infty$, includes axial flow and hence three-dimensional effects. As a consequence the Batchelor vortex is susceptible to a complicated variety of instabilities in different parameter regimes. Both exponential and algebraic inviscid instabilities are inherently three-dimensional: inviscid exponential instabilities are only active at small q, and the algebraic instability relies on the three-dimensionality of the mean flow (see § 4.4 of Heaton & Peake (2006) for details). Given the inviscid nature of the dominant transient mechanism found in § 4, the weaker viscous exponential instabilities are not expected to play as important a role over the time scales in which the inviscid mechanisms are active. The role of the inviscid instabilities will be important as we reduce q from ∞ to investigate three-dimensional vortices, and so before proceeding to the transient growth results we present here, for convenience, a brief review of the relevant inviscid instabilities and their stability boundaries.

The inviscid modal instabilities, which correspond to complex eigenfrequencies and exponential growth in time, are the strongest instabilities. When $Re<\infty$ the growth rates of these inviscid instabilities are reduced, and for sufficiently small Re the growth rate reduces to zero and the instability becomes stabilized. For the weakest inviscid instabilities this may occur at high values of Re, but for the strongest inviscid instabilities with the largest growth rates such stabilization does not occur at the Reynolds numbers of interest (e.g. for $m=-1$ the strongest inviscid instability persists down to $Re=14$, Lessen & Paillet 1974). For all the Reynolds numbers of aerodynamic interest, then, exponentially growing instabilities exist, but they do not always satisfactorily explain breakdown, because they are restricted to somewhat small values of the swirl parameter q. Figure 5 shows the inviscid stability boundaries of the Batchelor vortex for $m=-1,-2$, determined by the method of Heaton (2007). The modal instabilities are confined to the shaded regions in the figure, restricted to swirl values $q<2.31, 2.11$ for $m=-1,-2$ respectively. For $m\leqslant -3$ these instabilities are

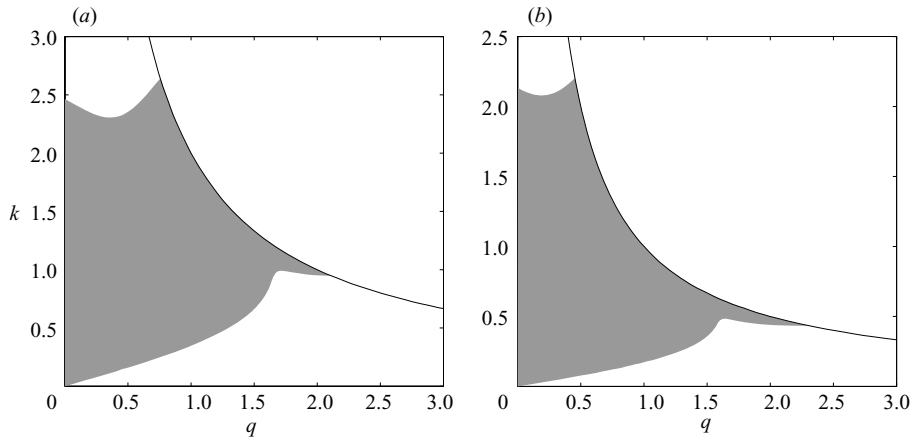

FIGURE 5. The inviscid temporal stability boundaries for the Batchelor vortex in the (q, k)-plane (*a*) $m = -2$, (*b*) $m = -1$. The shaded region has exponential modal instability. The solid line shows the boundary of the algebraically unstable region, $k < |m|/q$.

restricted to yet smaller q (Stewartson & Brown 1985). Finally, note that the narrow tongue of unstable modes with the largest q (approximately $q \geqslant 1.6$ for $m = -1, -2$ in figure 5) are all very weak (see Heaton 2007). As a consequence the modes in this tongue are stabilized, as Re is reduced from infinity, well before the bulk of the unstable region at smaller q.

The Batchelor vortex is algebraically unstable according to the theory of Heaton & Peake (2006) when $Re = \infty$ and the exponent given by (4.5) has $\sigma(r) > 0$, which corresponds to

$$kq(kq + m) < 0. \tag{5.2}$$

For these cases the continuous spectrum causes point-wise algebraic growth for large times in the regions below the solid lines in figure 5.

5.2. *Transient growth trends at high Re*

The exponent $\sigma(r)$ for the Batchelor vortex scaled on the swirl velocity, as given by (5.1), is found using (4.5) to be

$$\sigma(r) = -\frac{1}{2} + \sqrt{\frac{1}{4} - \frac{(1 - \mathrm{e}^{-r^2})\,\mathrm{e}^{-r^2} k(k + mq^{-1})}{r^4[-kq^{-1}\,\mathrm{e}^{-r^2} + mr^{-4}(-1 + \mathrm{e}^{-r^2}(1 + r^2))]^2}}. \tag{5.3}$$

This implies that

$$\sigma(r) \sim \frac{1}{r}\frac{\sqrt{-k(k + mq^{-1})}}{|kq^{-1} + m/2|} \tag{5.4}$$

as $r \to 0$. The inviscid Batchelor vortex is therefore a flow for which $\sigma_{\max} = \infty$. For $q > 2.31$ the inviscid vortex has no exponential instabilities (Stewartson & Brown 1985; Heaton 2007), so we expect the continuous spectrum effects illustrated by the problems considered in § 4 to provide transient growth. The simple scaling (4.9) of § 4 involving a finite $\sigma_{\max}$ cannot apply, but we will nevertheless hope to use the understanding gained from those simpler cases. In fact, algebraic growth for which $\sigma_{\max} = \infty$ must formally correspond to growth faster than any power of t, suggesting a strong transient effect in this case. At times short enough for accurate numerical calculation (as in figure 6) the gain has been observed to grow algebraically (i.e. slower

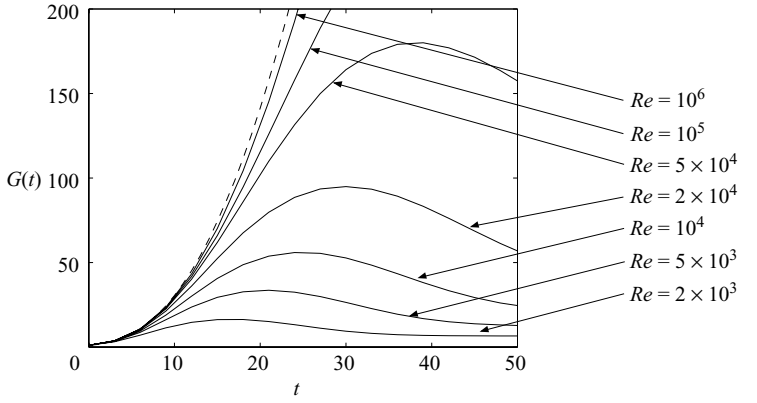

FIGURE 6. An illustrative collection of gain curves $G(t)$ for a Batchelor vortex with $(m, q, k) = (-2, 3, 0.3)$. Solid lines represent various viscous cases, and the dashed line shows the inviscid case ($Re = \infty$).

than exponentially), with an exponent which is gently increasing as time proceeds. As ever, the algebraic instability is formally absent for $Re < \infty$, but its effect can still be felt at finite Reynolds numbers, as we now discuss.

The link between the inviscid and finite-Re problems was discussed earlier, and let us revisit it now in the specific context of the Batchelor vortex. The important instabilities are expected to be inviscid in character, and hence damped by the inclusion of viscosity. The basic phenomenon which we wish to highlight is that the inviscid case provides an upper bound or envelope for the significant transient growth at finite Re. An example of this for the Batchelor vortex is shown in figure 6, and similar plots showing the same behaviour have been given for plane Couette flow (figure 7 of Trefethen *et al.* 1993) and compressible boundary layer flow (figures 1 and 2 of Hanifi & Henningson 1998). The example shown in figure 6 is one which possesses the algebraic instability, but no modal instability, when $Re = \infty$. For $Re < \infty$ the inviscid algebraic behaviour is seen to translate into a transient growth as anticipated. For approximately $Re > 10^5$ a viscous instability is present (see figure 4 of Fabre & Jacquin 2004), and was present in our numerics, but it is found not to affect the 'enveloping' behaviour of the viscous gain curves by the inviscid curve at these times. Only for very large times will the weak exponential growth of the viscous mode (the growth rate is less than 0.02 in figure 6, and in general scales as $\sim Re^{-1/3}$: see Le Dizès & Fabre 2006) overtake the algebraic transient effect.

For other cases (e.g. small q) there may be exponentially unstable inviscid modes, meaning stronger exponential growth of $G(t)$ which will persist until the Reynolds number is lowered below a critical value. For Re above the critical value, $G(t)$ would grow as $t \to \infty$ and not eventually decay, while still being enveloped by the inviscid gain. Therefore, to summarize, for all cases the statement that the inviscid results control the transient growth at large but finite Re is justified. The only proviso is that if an unstable viscous mode is present then it will take over from the inviscid effects after longer times, but we are primarily interested here in the fast growth possible over short times. To quantify these transient effects directly, we will now concentrate on a single finite Reynolds number. We will find that the general trends, which we have described by a combination of inviscid continuous spectrum theory and viscous damping via shear diffusion, are modified by some more specific effects.

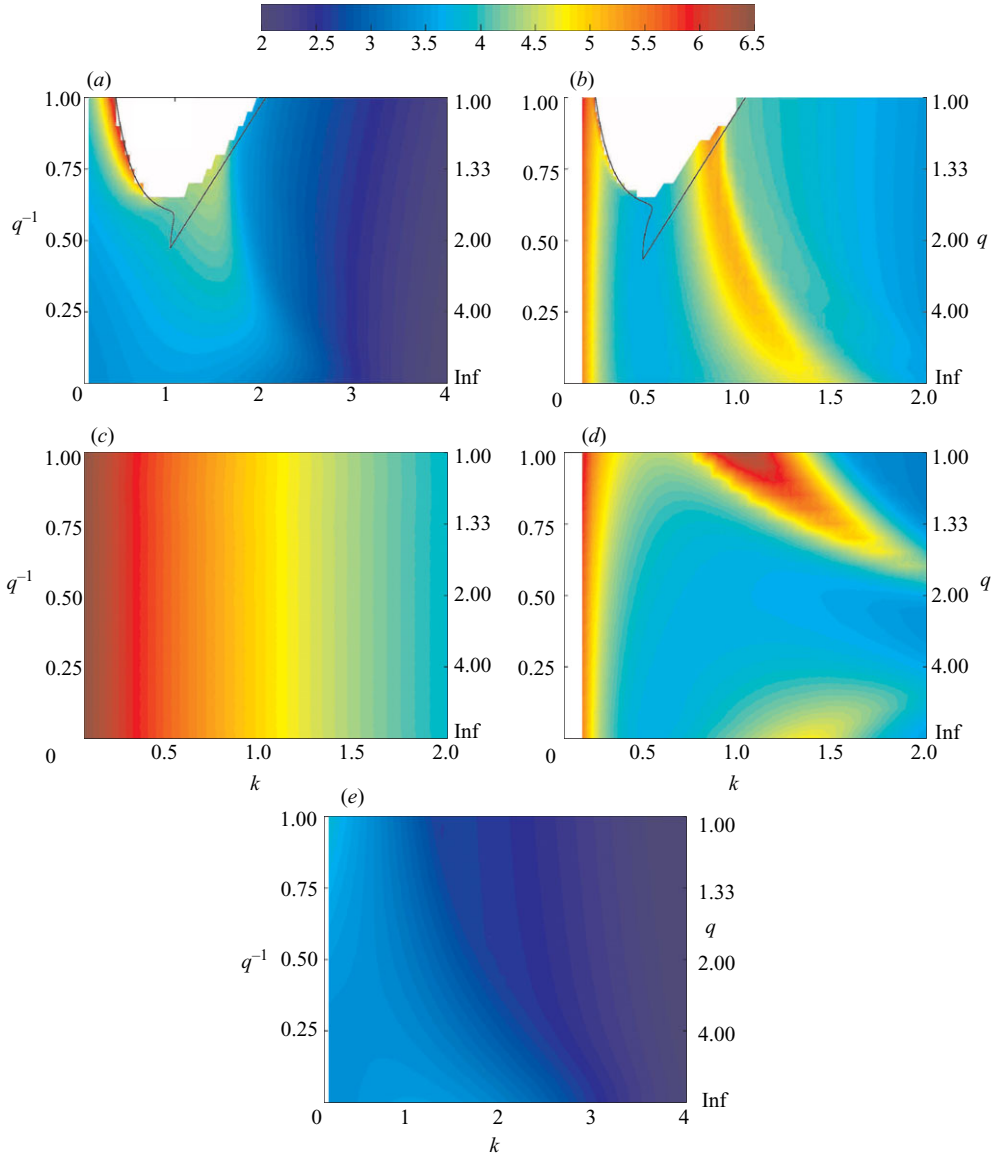

FIGURE 7. Plots showing $\log(G_{\max})$ for $Re = 5000$, (*a*) $m = -2$, (*b*) $m = -1$, (*c*) $m = 0$, (*d*) $m = 1$, (*e*) $m = 2$. The colour scale is given by the bar at the top. In (*a*) and (*b*) the regions above the solid lines are the inviscidly modally unstable regions.

5.3. *Transient growth at* $Re = 5000$

We now present the detailed results of our viscous transient growth calculations. Figure 7 shows the quantity $\log(G_{\max})$ for $-2 \leqslant m \leqslant 2$ and $Re = 5000$ in the (k, q^{-1}) -plane. We plot values of the swirl parameter $1 \leqslant q \leqslant \infty$, corresponding to $0 \leqslant q^{-1} \leqslant 1$ on the ordinates of the plots. The Reynolds number used in the calculations was chosen to be sufficiently large to be physically relevant, but also within the numerical limitations of our code. Larger Re can be treated in some cases, but higher values require more careful monitoring of numerical tolerances as well as more CPU time. Figure 6 and the discussion above, and also the results of Antkowiak & Brancher

(2004) and Pradeep & Hussain (2006) for varying Re, suggest that the same trends will translate to higher Re. We indicate in figures 7(a) and 7(b) the region of the plane which is *inviscidly* exponentially unstable. For $Re = 5000$ the exponential instabilities occupy a smaller region which is shown up by the blank portion of the figures: for these parameters $G(t)$ is unbounded and has no maximum value to plot. Note that, as anticipated, the inviscid modes at larger q are the most readily stabilized at finite Re. For the parameters in figure 7 there are no viscous instabilities present: see Fabre & Jacquin (2004) for the computed neutral curves of the viscous instabilities, and note that their definition of Re is different from ours. We argued above that viscous instabilities would not affect the large transient gains which occur at comparatively early times. Their effect at long times would complicate the plots of $G_{\max}$, however, so it is best here to choose parameters for which they are absent.

The first comment to make about the plots in figure 7 is that for $q = \infty$ the results along the abscissa of each plot recover the results of Pradeep & Hussain (2006) (see their figures 14a and 19). As was mentioned in § 3.3, recovering Pradeep & Hussain's results and also those of Antkowiak & Brancher (who, note, use a different definition of Re), on setting $q = \infty$ was the most important validation of our numerical code. As for the Lamb–Oseen vortex, and also for the ducted vortices of § 4, the Batchelor vortex shows strong transient effects. However, we now have a more complicated flow with $\sigma_{\max} = \infty$, the presence of exponential instabilities, and an unbounded flow domain. Each of these will be seen to modify and complicate the results beyond the simple general discussions of § 4.

Let us examine the results in figure 7 in detail. Now, the gain in the case of the Lamb–Oseen vortex is the same for m and $-m$ (see Pradeep & Hussain 2006), but we immediately see that for the Batchelor vortex the non-zero axial flow breaks this symmetry and the results are quite different. For $m = -2$ figure 7(a) shows that the possible transient growth gradually increases as q is lowered, meaning that the axial component of the mean flow is increased and the mean flow is made more strongly three-dimensional. We suggest that this increase in $G_{\max}$ is due to increased proximity to the inviscidly unstable regions of the (k, q)-plane, causing $G(t)$ to grow faster (see the discussion of figure 8 at the end of this subsection for more details). In contrast to figure 7(a), figure 7(e) shows no such increase when $m = 2$ and the inviscid instabilities are absent. The results for $|m| > 2$ will be qualitatively similar to the $|m| = 2$ case, but with decreasing growth for larger $|m|$ due to the increased action of viscous diffusion on the finer scales of the higher-order disturbances. The results for $|m| \leqslant 1$ are quite different, however.

First consider $m = \pm 1$, also called the bending or helical modes. Overall, the most significant discovery from the studies of the Lamb–Oseen vortex ($q = \infty$) is a 'resonance' for $|m| = 1$ at $k \simeq 1.3$, where $G_{\max}$ has a maximum. A resonance explanation for this maximum is suggested by Antkowiak & Brancher (2004) and discussed in more detail by Pradeep & Hussain (2006). According to Pradeep & Hussain, the potential resonance is between (a) advection and tilting of unsteady vorticity by the mean-flow swirl, and (b) a vorticity core mode localized on the symmetry axis. This resonance should occur if the mean-flow angular velocity advecting the unsteady vorticity matches the frequency of a core mode. Further, the initial condition for this transient growth is localized at the finite 'ribbon radius' at which the mean flow has the required angular velocity (Pradeep & Hussain 2006), and so could be a physically feasible initial condition (as discussed at the end of § 3.1). In figure 7(b) the maximum in $G_{\max}$ observed for the Lamb–Oseen vortex at $k \simeq 1.3$ persists and strengthens (and moves to smaller k) as the axial flow in the vortex is increased. For $Re = 5000$ the

strength of the resonance in figure 7(*b*) is doubled by the inclusion of the axial flow, which we attribute to the proximity of inviscid instabilities (see the discussion of figure 8 at the end of this subsection for more details). In contrast for $m = +1$ the resonance dies away when q is lowered, probably because there is no inviscid instability off which to feed. The $m = 1$ modes show some strong growth for smaller swirl, $q \lesssim 1.4$, but this must be interpreted as unimportant: for these values of q the mean flow has strong exponential instabilities at $m < 0$. Recall that our primary interest is whether transient mechanisms can play a role for $q \gtrsim 2$, the physically important regime in which strong exponential instabilities do not immediately explain breakdown. Therefore the persistence of the resonance for $m = -1$ as q^{-1} is increased from zero is the more important result.

Let us briefly look more closely at the peak in $G_{\max}$ at $q = \infty$, $k \simeq 1.3$ in the bending modes. The arguments given by Pradeep & Hussain (2006) to support a resonance use simplified model equations intended to capture the important mechanisms for a vortex without axial flow. For this reason it is worth confirming that their resonance mechanism is at play here in the full problem. Taking our cue from figure 7(*b*) we investigated the case of $Re = 5000$, $m = -1$, $q = 4$ and $k = 1.05$. The optimal initial condition is found to be localized around a finite radius r_0 as expected, with $r_0 = 2.9$ in this case. The value of r_0 was also found to be constant as Re increases, in line with Pradeep & Hussain's prediction. To determine whether there is a resonance or not, we calculated the temporal frequency spectrum of the Batchelor vortex for the same parameters. The two principal (i.e. least damped) core modes in the spectrum have oscillation frequencies $Re(\omega) = 0.355$ and 0.116, which imply resonant radii (where the mean-flow angular velocity matches $Re(\omega)$) of $r_0 = 1.62$ and 2.94, respectively. The latter radius agrees very well with the results of the gain calculations, suggesting that the second core mode is indeed resonating with the advection and tilting of vorticity by the mean flow. This is the confirmation we seek, that the resonance mechanism outlined by Pradeep & Hussain (2006) is at play in the full problem for this flow.

The $m = 0$ axisymmetric disturbances are found to be unaffected by the axial flow (figure 7*c*). The growth levels for $m = 0$ appear at first glance to be large, although in fact they are not physically meaningful (as noted by Pradeep & Hussain 2006) because a very long time $t_{\max}$ is needed to achieve the maximum gain. Further, the optimal initial conditions have a spatial structure localized at large radii, which we consider to be infeasible in practice (it necessitates an unlikely coordination of conditions far from the vortex axis in all directions, and also likely violates the assumption of a single isolated vortex: see the end of § 3.1). In fact, formally, $G_{\max} \to \infty$ as $k \to 0$ when $m = 0$, a phenomenon which Pradeep & Hussain (2006) discussed: for $m = k = 0$ viscous diffusion does not act on any axial or azimuthal gradients in the disturbance field, a situation which can be exploited by optimal perturbations to achieve arbitrarily large growth. We mention this because it is evident from figures 7(*b*) and 7(*d*) that $G_{\max} \to \infty$ as $k \to 0$ for $m = \pm 1$ as well. In § 5.4 we will consider how physically meaningful that growth is, and also describe the mechanism (which is similar to the axisymmetric case) for the formal blow-up of $G_{\max}$.

The peculiar behaviour seen for $m = 0$ acts as a reminder that not only should we take note of the absolute gain attainable, but also the rate at which any growth accumulates. Gains which only accumulate extremely slowly should be interpreted as physically unlikely, whereas in the other extreme if two simultaneous growths are competing we should like to know which will grow faster. One possibility would be to plot the values of $t_{\max}$ corresponding to the maximum gains in figure 7, but this only conveys information about the single optimal perturbation at that Reynolds number.

Instead we recall figure 6 and use the gain of the inviscid vortex as a measure of how fast growth is likely to occur at any finite Re. Figure 8 shows the inviscid gain at $t = 15$ for the same values of m for which we have calculated and discussed the maximum gain at $Re = 5000$. The chosen time $t = 15$ (recall that time is scaled on the vortex swirl velocity) is of the same order of magnitude as $t_{\max}$ for much of the presented gains at $Re = 5000$, though it is shorter than the time associated with the $m = -1$ resonance in figure 7(b), which typically has $t_{\max} \simeq 100$. A snapshot of the inviscid growth at this time should be directly helpful in interpreting figure 7. For example from figure 8(c) it is immediately clear that any growth at $m = 0$ must be extremely slow, for any Re, and so this quickly confirms the statement that the large $G_{\max}$ values in figure 7(c) are misleading. Note that this also agrees with the observation made in § 4.2 that for $m = k = 0$ the inviscid problem simplifies to a normal operator and has $G(t) \equiv 1$: by continuity of $G(t)$, for fixed t, as a function of k and q, the $m = 0$ gain (at fixed t) must be small for a small k. For the non-axisymmetric modes the fastest inviscid growth is of course seen in the inviscidly unstable regions, due to the algebraic and especially the exponential instabilities. Because $G(t)$, for fixed t, must be a continuous function of k and q, increased proximity to the inviscidly unstable regions of the (k, q)-plane implies a larger inviscid gain in general. In the viscous problem proximity to the inviscidly unstable regions therefore translates to faster-growing gain, and, assuming $t_{\max}$ is roughly constant, tends to give larger maximum gain $G_{\max}$. This is the suggested explanation for the general trend of increasing $G_{\max}$ as q decreases seen in figures 7(a) and 7(b). Note that the fast growth for $m > 0$ in figures 8(d) and 8(e) at small k is due to the $(-m, k) \leftrightarrow (m, -k)$ symmetry in the problem: the small-k gain for $m > 0$ must match continuously onto the small-k gain for $m < 0$ at finite time t. Comparing the various plots, the most notable feature of the inviscid gains is that the small-k limit for $m = \pm 1$ is clearly not the same as the small-k limit for $m = 0$. The growth rates for the long-wave bending modes are much faster, due to the proximity of the inviscid instabilities, both algebraic and exponential. This further motivates us to take a close look at the $k \to 0$ limit of the bending modes, to determine whether or not the large maximum gains in figures 7(b) and 7(d) are physical.

5.4. *The long-wavelength bending modes*

To understand why $G_{\max} \to \infty$ as $k \to 0$ for $m = \pm 1$ we shall inspect the viscous terms on the right-hand side of (2.3)–(2.5). Setting $k = 0$, we obtain

$$\frac{\partial u}{\partial t} + \cdots = \frac{\nu}{r^2}[-m^2 u] + \frac{\nu(ru')'}{r}, \tag{5.5}$$

$$\frac{\partial v}{\partial t} + \cdots = \frac{\nu}{r^2}[-(1 + m^2)v - 2\mathrm{i}mw] + \frac{\nu(rv')'}{r}, \tag{5.6}$$

and

$$\frac{\partial w}{\partial t} + \cdots = \frac{\nu}{r^2}[-(1 + m^2)w + 2\mathrm{i}mv] + \frac{\nu(rw')'}{r}, \tag{5.7}$$

respectively. Note that the terms on the right-hand side not in square brackets correspond to the action of viscosity through radial variations of the unsteady flow. For $m = 0$ we see that the term in square brackets on right-hand side of (5.5) vanishes, meaning the only viscous diffusion acting on u is due to radial variations. This situation can be exploited by optimally chosen initial conditions which vary over arbitrarily long radial scales, in order to bypass viscous damping and produce an arbitrarily large gain. This is the situation described by Pradeep & Hussain (2006)

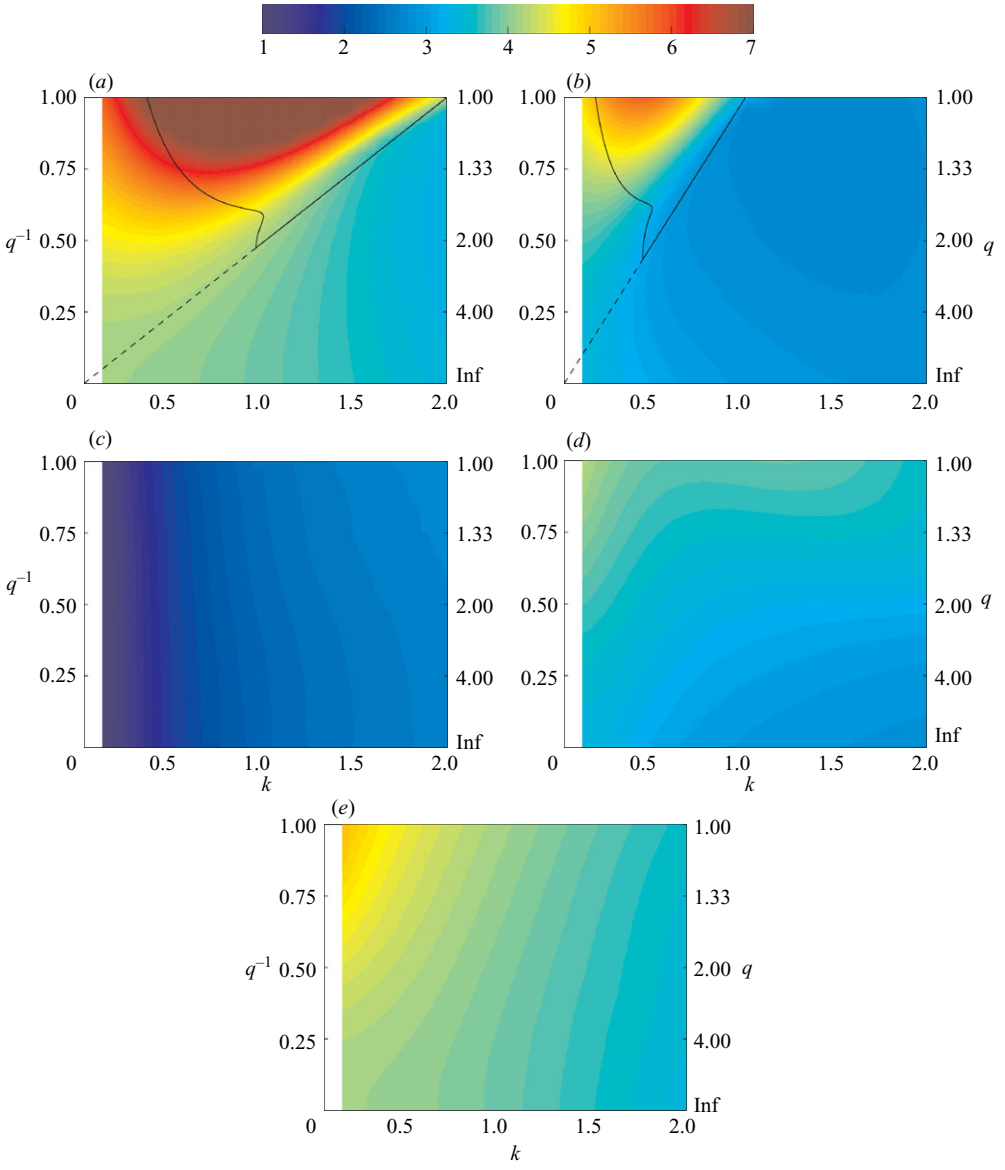

FIGURE 8. Plots of $\log(G(t=15))$ for $Re=\infty$, (*a*) $m=-2$, (*b*) $m=-1$, (*c*) $m=0$, (*d*) $m=1$, (*e*) $m=2$. The colour scale is given by the bar at the top. In (*a*) and (*b*) above the solid lines are the inviscidly modally unstable regions; above the dashed lines (which continue coincident with the straight portion of the solid lines) the inviscid flow is algebraically unstable.

to explain the peculiar $m=0$ growth. Note, however, that Pradeep & Hussain used a different argument, based on a simplified model equation intended to capture the relevant mechanisms for an $m=0$ mode, to reach this conclusion. Of course, in practice the assumed mean flow will not hold at very large radii because of nearby bodies or flow non-uniformities, meaning that optimal initial conditions needing arbitrarily long length scales are infeasible.

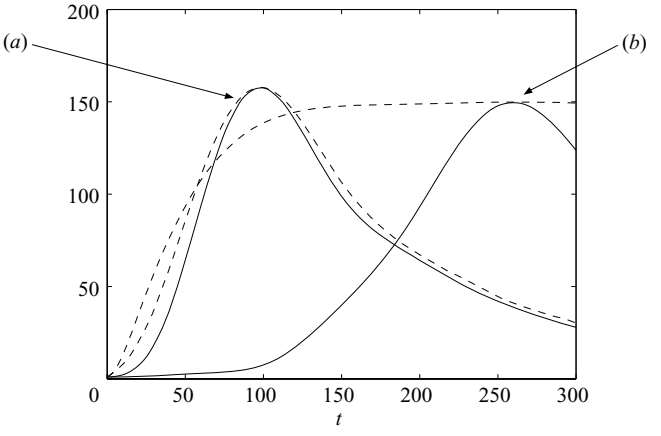

FIGURE 9. Gain curves $G(t)$ (dashed lines) and the energy amplification curves $E(t)/E(0)$ for the optimal perturbation (solid lines) for $Re = 5000$, $m = -1$, $q = 4$ and (*a*) $k = 1.05$, (*b*) $k = 0.13$.

Considering $m = \pm 1$, a similar phenomenon occurs, only now masked by the choice of dependent variables. Taking a linear combination of (5.6) and (5.7) one obtains

$$\frac{\partial}{\partial t}\{(1+m^2)w + 2imv\} + \cdots = \frac{\nu}{r^2}[-(1-m^2)^2 w] + \frac{\nu}{r}(r((1+m^2)w + 2imv)')'. \quad (5.8)$$

So for $m^2 = 1$ the viscous terms in square brackets in (5.8) vanish, and again one component of the disturbance velocity does not feel the action of viscous diffusion, except through radial variations. Thus the formal blow-up of $G_{\max}$ as $k \to 0$ is explained for the bending modes, and the large growth relies on initial conditions which may be physically infeasible, as in the axisymmetric case.† However, we still have the dilemma that this conclusion is not fully consistent with figures 8(*b*) and 8(*d*): the growth rate for any transients should be reasonable for small-k bending modes, and indeed faster than the growth rates involved in the bending mode resonance, suggesting that some meaningful small-k growth *should* be possible.

This is explored further in figure 9, where we take $Re = 5000$, $m = -1$ and $q = 4$ and consider two distinct axial wavenumbers which have approximately the same value of $G_{\max} \simeq 150$. The first wavenumber $k = 1.05$ is the case considered above, for which it was confirmed that a bending mode resonance is present. The second wavenumber $k = 0.13$ is small and has a maximum gain which utilizes the mechanism described in this subsection to bypass some of the action of viscosity. This is confirmed by observing that the gain curve in figure 9(*b*) is extremely flat (so flat that the maximum is hard to discern by eye). For this small value of k viscosity acts extremely weakly on axial and azimuthal gradients, and the optimal perturbation is able to take a form such that the viscous damping occurs on a very long time scale, leading to the flat gain curve in figure 9(*b*) which after its maximum decays to zero very slowly. The solid lines showing the energy amplification $E(t)/E(0)$ for the optimal perturbations in figure 9 show how dramatically different the two cases are, despite achieving roughly the same total gain. The energy of the $k = 0.13$ optimal grows slowly at first, and is still less than 10 by the time that the $k = 1.05$ optimal has attained its

† Note that the effect described can only apply to unbounded flows. Accordingly, $G_{\max}$ is finite as $k \to 0$ for Hagen–Poiseuille flow: see Schmid & Henningson (1994)

maximum gain. However, it is clear that the gain curve for $k = 0.13$ does not grow so slowly at first: a feature we anticipated from figure 8(*b*), and which results from the presence of the algebraic instability at those parameters when $Re = \infty$. The small wavenumbers *can* grow quickly for $m = \pm 1$ because of the proximity of the inviscid instabilities in parameter space, but this point is hidden if we only look at the optimal perturbations at a finite Re, because the optimal perturbation can grow a little more by taking a very much longer time to do so. So, what level of growth is possible for the $k = 0.13$ case if we wish (*a*) that the initial condition has a physically feasible spatial structure, and (*b*) the time scale for the growth is not too long for the effect to be meaningful? The optimal perturbation of figure 9(*b*) is localized (where, rather loosely, we define this to mean the position where $|\boldsymbol{u}|$ is greatest) at $r_0 = 6.11$, and for larger Re this value will increase. The natural comparator is the resonant case, for which the resonant radius was $r_0 = 2.9$. In comparison to this the $k = 0.13$ disturbance can have gain $G(40) = 77$ (half of the optimal) before its initial condition is localized at a larger radius. Further, almost all of the optimal gain can be achieved for initial conditions which are localized at comparable radii. This is because the two gain curves in figure 9 are comparable for $t \lesssim 100$ and most of the gain for $k = 0.13$ can be achieved at short times, without having to resort to exploiting the potentially weak viscous damping. Thus we conclude that the small-k bending mode disturbances are capable of contributing significant transient growth, although this is at first glance hidden by the raw results for $G_{\max}$ and $t_{\max}$. It seems, at least for the example we have considered in detail, that the small-k effect will be comparable to the resonant effect. Consideration of the inviscid growth rates in figure 8 suggests that this trend should continue for larger Reynolds numbers.

6. Conclusions

We have investigated numerically the level of transient growth possible in vortices with axial flow. We considered a family of ducted vortices in § 4 which are commonly used to model aeroengine flows, and in § 5 the Batchelor model of a trailing line vortex. Substantial transient growth was found to be possible in both cases. In line with previous investigators we found that the primary mechanism for the transient growth is inviscid. More specifically, for flows without any strong exponential instabilities, we attribute it to be a continuous spectrum effect (with Landahl's lift-up effect being a special case of the continuous spectrum effect when streamwise wavenumber is zero). In § 4 we explored the inviscid mechanisms in detail. Heaton & Peake (2006) found that inviscid swirling flow can have an unstable continuous spectrum which is stronger than that for two-dimensional or non-swirling flows. The wider range of responses from the continuous spectrum in swirling flow – compare (4.5) and (4.12)– was found to lead to a wide range in the transient effects (figure 3). The quantity $\sigma_{\max}$, derived from the inviscid continuous spectrum theory, appears in a new scaling (4.9) for the increase of transient growth with time, the familiar quadratic scaling for non-swirling flows now being interpreted as the special case $\sigma_{\max} = 0$. This, combined with the appropriate viscous damping time scale, then gives the scaling for the optimal transient growth.

For the specific case of the Batchelor vortex we performed detailed calculations for one representative vortex Reynolds number, $Re = 5000$, and discussed how the results will translate to higher values. The general effects we have discussed are modified by several complications in this case, but it was nevertheless found that the inviscid case (for which there is good theoretical understanding of the various instabilities

and their boundaries) is of use in understanding the viscous transient growth. The results show that stronger growth is possible for the Batchelor vortex than for the Lamb–Oseen vortex, as expected given the three-dimensional nature of the inviscid instabilities. The Lamb–Oseen vortex itself only has the effect of the swirl, leading to lesser but still significant transient growth.

The detailed results show that for $|m| = 2$ no significant transient gain can be attained, except in the immediate proximity of the unstable parameters at low swirl levels. It is expected that for $|m| > 2$ the same trend will continue, with even smaller gains because of the increased action of viscous damping on the higher-order modes. For $|m| \leqslant 1$ the situation is more complicated, however, and some care was needed in correctly interpreting the results. In agreement with the findings of Pradeep & Hussain (2006) for the Lamb–Oseen vortex, the $m = 0$ modes have very large theoretical transient gains, however they are not physically important: the gain accumulates extremely slowly, and also the required initial conditions must vary over longer and longer length scales for increasing Re. This is unlikely to be triggered in a real flow because, far from the vortex core, the assumption of a single isolated vortex will fail. Indeed, it also seems unlikely such an initial condition will be created by random noise because of the coordination needed in all directions far from the vortex core (note, however, that full investigation of how successfully stochastic forcing excites transient growth requires a different analysis: see Farrell & Ioannou 1993). By considering the inviscid vortex it was confirmed that no significant transient growth can be attained for $m = 0$, at any Re, and so transient mechanisms are evidently not involved in the 'bubble' form of vortex breakdown. The $m = \pm 1$ bending modes, however, do show promising levels of transient growth. For $m = -1$ a resonance is found which generates large transient growth. This effect was first found in the studies of the two-dimensional Lamb–Oseen vortex (Antkowiak & Brancher 2004; Pradeep & Hussain 2006), and we observed that it persists and strengthens with the inclusion of axial flow in the vortex core. We also confirmed, using the full Navier–Stokes equations, that such a resonance mechanism is present here. For $m = \pm 1$ we also showed that the limit of vanishing axial wavenumber allows arbitrarily large maximum gain, a formal result which is only possible for unbounded flows due to the increasing length scale of the corresponding optimal initial condition. As for $m = 0$ the (formal) infinite gain is not physically important, but unlike the axisymmetric modes the small-k bending modes *can* still produce significant transient effects. This was seen by consideration of the inviscid vortex, which controls the rate of growth, but the result is somewhat hidden by the raw viscous results. If we restrict consideration to initial conditions which are comparable to those associated with the resonance, and also time scales no longer than that of the resonance, then we find the small-k bending modes should show a transient effect of approximately the same importance as the resonance.

Overall, the bending modes show significant possible growth via transient effects. A resonance effect between the mean swirl and a vorticity core mode, and also a long-wavelength effect, can generate comparable gains at comparable rates. Therefore this provides another potential route to the 'spiral' form of vortex breakdown which is observed at swirl values $q \simeq 2$, for which the only long-time instabilities are weak viscous modes. At least two important further questions must be addressed to test whether breakdown may be initiated by such transient growth. First, the mean-flow profile used in our calculations, and as used by almost all other investigators, is only the leading term in Batchelor's similarity solution. At higher order (in Re^{-1}) the flow may be more complicated, being non-parallel and unsteady, and whether this significantly alters the results at the Reynolds numbers of interest is not known.

The mean flow should vary on the $O(Re)$ time scale of viscous diffusion, whereas the optimal growth in figure 7 occurs at $t_{\max} = O(Re^{1/3})$ on the faster shear-diffusion time scale. Hence, it is formally justified as $Re \to \infty$ to use the steady mean-flow approximation, but the Reynolds numbers of interest are only moderately large, so this effect could alter the results. Second, whether the transient effects we have presented are enough to trigger nonlinear effects is an important question that cannot be answered by a purely linear analysis, and probably requires DNS calculations to resolve. The present results support the conclusions of Antkowiak & Brancher (2004) and Pradeep & Hussain (2006) for two-dimensional vortices that the transient growth route to breakdown is a possibility, and we believe this requires further investigation.

The authors thank Dr A. J. Cooper for kindly sharing some unpublished results relating to § 4. CJH is grateful to Trinity College, Cambridge, for its financial support.

Appendix A. The linear operators $\mathscr{A}$, $\mathscr{L}$, $\mathscr{M}$ and $\mathscr{N}$

We give here the details of the various linear differential operators which appear in the evolution equation (2.8) and the transient growth theory of § 3.2. First we have

$$\mathscr{A} = \begin{pmatrix} \dfrac{\mathrm{i}}{kr}\dfrac{\mathrm{d}}{\mathrm{d}r}r & -\dfrac{m}{kr} \\ \mathscr{I} & 0 \\ 0 & \mathscr{I} \end{pmatrix}, \tag{A 1}$$

where $\mathscr{A}$ recovers the unsteady velocity from the state variable $\boldsymbol{v}$ of the optimization problem, i.e. $\boldsymbol{u} = \mathscr{A}\boldsymbol{v}$. Note that $\mathscr{I}$ is the identity operator, and all operators act to the right. The adjoint with respect to the inner product (2.10), $\mathscr{A}^\dagger$, can be obtained by making use of

$$\left(\frac{\mathrm{d}}{\mathrm{d}r}\right)^\dagger = -\frac{1}{r}\frac{\mathrm{d}}{\mathrm{d}r}r, \tag{A 2}$$

and is found to be

$$\mathscr{A}^\dagger = \begin{pmatrix} \dfrac{\mathrm{i}}{k}\dfrac{\mathrm{d}}{\mathrm{d}r} & \mathscr{I} & 0 \\ -\dfrac{m}{kr} & 0 & \mathscr{I} \end{pmatrix}. \tag{A 3}$$

The adjoints of the other operators (not reproduced here) can be similarly written down by using (A 2).

The operators appearing in the evolution equation (2.8) are given by

$$\mathscr{L} = \begin{pmatrix} \dfrac{\mathrm{i}m}{kr^2}\dfrac{\mathrm{d}}{\mathrm{d}r}r & -\dfrac{\Delta}{kr^2} \\ \dfrac{\mathrm{i}}{k}\dfrac{\mathrm{d}}{\mathrm{d}r}\dfrac{1}{r}\dfrac{\mathrm{d}}{\mathrm{d}r}r - \mathrm{i}k & -\dfrac{m}{k}\dfrac{\mathrm{d}}{\mathrm{d}r}\dfrac{1}{r} \end{pmatrix}, \tag{A 4}$$

$$\mathscr{M} = \begin{pmatrix} \dfrac{k(Wr)' - mU'}{r} + \dfrac{m\Gamma}{kr^2}\dfrac{\mathrm{d}}{\mathrm{d}r}r & \dfrac{\mathrm{i}\Delta\Gamma}{kr^2} \\ \dfrac{1}{k}\dfrac{\mathrm{d}}{\mathrm{d}r}\dfrac{\Gamma}{r}\dfrac{\mathrm{d}}{\mathrm{d}r}r - k\Gamma - \dfrac{\mathrm{d}}{\mathrm{d}r}U' & \dfrac{\mathrm{i}m}{k}\dfrac{\mathrm{d}}{\mathrm{d}r}\dfrac{\Gamma}{r} - \dfrac{2\mathrm{i}kW}{r} \end{pmatrix}, \tag{A 5}$$

and

$$\mathscr{N} = \begin{pmatrix} -\dfrac{2\mathrm{i}mk}{r^2} & -\dfrac{k}{r}\dfrac{\mathrm{d}}{\mathrm{d}r}r\dfrac{\mathrm{d}}{\mathrm{d}r} + \dfrac{k(1+\Delta)}{r^2} \\ \dfrac{\mathrm{i}k(1+\Delta)}{r^2} - \dfrac{\mathrm{i}k}{r}\dfrac{\mathrm{d}}{\mathrm{d}r}r\dfrac{\mathrm{d}}{\mathrm{d}r} & -\dfrac{2mk}{r^2} \end{pmatrix} + \begin{pmatrix} \dfrac{m}{r^2}\dfrac{\mathrm{d}}{\mathrm{d}r}r\dfrac{\mathrm{d}}{\mathrm{d}r} - \dfrac{m\Delta}{r^3} \\ \dfrac{\mathrm{d}}{\mathrm{d}r}\dfrac{1}{r}\dfrac{\mathrm{d}}{\mathrm{d}r}r\dfrac{\mathrm{d}}{\mathrm{d}r} - \dfrac{\mathrm{d}}{\mathrm{d}r}\dfrac{\Delta}{r^2} \end{pmatrix} \times \begin{pmatrix} \dfrac{\mathrm{i}}{kr}\dfrac{\mathrm{d}}{\mathrm{d}r}r & -\dfrac{m}{kr} \end{pmatrix}. \tag{A 6}$$

To abbreviate the algebra we have defined

$$\Delta = m^2 + k^2r^2, \tag{A 7}$$

$$\Gamma = Uk + Wm/r \tag{A 8}$$

and not expanded the matrix product (shown by $\times$) in (A 6).

Appendix B. Inviscid transient growth from the continuous spectrum: the t^2 result

B.1. *Neutral continuous spectra*

In this appendix we discuss the gain curve $G(t)$ for an inviscid flow without exponential instabilities. First consider a flow in which the continuous spectrum is neutrally stable, a simple building block from which we can infer the gain in more complicated flows. The characteristic behaviour we wish to explain is that in general

$$G(t) \sim t^2 \tag{B 1}$$

as $t \to \infty$ for such flows, the mechanism for which is inherently a continuous spectrum effect.

To begin, consider two distinct frequencies, say ω and $\omega' \equiv \omega + \Delta\omega$, which are both members of the continuous spectrum C_ω, as defined by (4.3) for a swirling flow or (4.11) for a two-dimensional flow. Note that we are free to take $\Delta\omega$ as small as we like, and we will use this to exploit the non-normality of the linearized equations and generate transient growth. The idea is that the two velocity eigenfunctions associated with ω and ω' are not orthogonal, and indeed are increasingly parallel as $\Delta\omega \to 0$. We pick an initial state containing a linear combination of the two eigenfunctions, each normalized in some sensible way, such that they efficiently cancel each other out. At later times the cancellation which occurs in the initial conditions will disappear, as we shall see, giving rise to transient growth. The initial conditions which give rise to the eigenfunctions for ω and ω' will differ only at $O(\Delta\omega)$. Hence, by choosing a suitable linear combination of the two (e.g. the difference) in which they efficiently cancel each other out, the initial kinetic energy can be as small as

$$E(0) = O(\Delta\omega^2). \tag{B 2}$$

At later times when $t = O(\Delta\omega^{-1})$, however, the two eigenfunctions will not cancel each other out, because they become fully uncorrelated due to the phase difference in the $\exp(-\mathrm{i}\omega t)$ time dependence. Hence the kinetic energy becomes

$$E(t) = O(1), \quad \text{for } t = O(\Delta\omega^{-1}). \tag{B 3}$$

The process described leads to the expected level of gain, $G(t_*) = O(t_*^2)$, where we have set $t_* = \Delta\omega^{-1}$. For longer times the maximum energy gain is achieved by taking smaller $\Delta\omega$, meaning increasingly proximate pairs of frequencies in the continuous spectrum.

B.2. *An example calculation*

In order to provide a more explicit demonstration of our argument, we will show how the mechanism described above applies to a simplified model system. The evolution of initial conditions according to the linearized Euler equations includes a contribution from the continuous spectrum C_ω for all but the most simple mean flows. The contribution of C_ω is obtained analytically by taking a Fourier–Laplace transform, solving the resulting system of ordinary differential equations and then inverting the transform in the usual way, with C_ω appearing as a branch cut in the inversion integrand (see Heaton & Peake 2006, for example). We will work here with the canonical form of a continuous spectrum contribution, but simplify the analysis by removing the spatial variables, leaving only time, and by restricting to a small one-parameter family of initial conditions.

Consider a quantity $\phi(t;\lambda)$, which is given at time $t=0$ by $\phi(0;\lambda)$, one of a family of initial conditions parametrized by the scalar λ. Suppose that $\phi(t;\lambda)$ evolves by the action of a linear operator which has a continuous spectrum C_ω, and an empty discrete spectrum. We can write

$$\phi(t;\lambda) = \oint_\Gamma \exp(-\mathrm{i}\omega t)\hat{\phi}(\omega,\lambda)\mathrm{d}\omega, \tag{B 4}$$

where Γ encircles C_ω in the complex-ω-plane and $\hat{\phi}(\omega,\lambda)$ is the function which would be obtained by solving the Fourier–Laplace transform of the linear system, subject to the initial conditions (parametrized by λ) and any appropriate boundary conditions. Recall that C_ω lies on a segment of the real-ω-axis, and that C_ω will be a branch cut for the function $\hat{\phi}(\omega,\lambda)$ in the complex-ω-plane. For the linearized Euler equations the canonical form (B 4) can be arrived at in a number of ways. For example, take a given mean flow, let ϕ stand for one component of the unsteady disturbance velocity and fix the values of r, k and m. Then the family of solutions given by the response to the impulsive forcing $\delta(r-\lambda)\delta(t+1)\,\mathrm{e}^{\mathrm{i}kx+\mathrm{i}m\theta}$ gives a useful family of solutions to consider. This particular example is of course a special case of the Green's function for the linearized Euler equations; a fully detailed calculation of a related Green's function, including continuous spectrum, can be found for comparison in Heaton & Peake (2006).

Working with the canonical form (B 4), we note that there must exist at least one frequency (and assume for simplicity that there is only one) $\omega_e(\lambda) \in C_\omega$ such that

$$\hat{\phi}(\omega,\lambda) = \begin{cases} O\left([\omega-\omega_e(\lambda)]^{-1}\right), & \text{as } \omega \to \omega_e(\lambda) \\ O(1) \text{ and smooth}, & \text{otherwise.} \end{cases} \tag{B 5}$$

This follows from our assumption that the continuous spectrum is neutrally stable and that $\sigma_{\max} = 0$. If $\sigma_{\max}$ were greater than zero a stronger singularity in the integrand $\hat{\phi}(\omega,\lambda)$ would be present on C_ω, giving rise to algebraic growth as $t \to \infty$. If a weaker singularity than (B 5) were present then $\phi(t;\lambda)$, as given by (B 4), would decay at large times and would not be neutrally stable. By standard methods (Lighthill 1958) it follows that at large times we have

$$\phi(t;\lambda) = \pi\mathrm{i}L(\lambda)\exp(-\mathrm{i}\omega_e(\lambda)t) + O(t^{-1}) \quad \text{for} \quad t \gg 1, \tag{B 6}$$

where

$$L(\lambda) \equiv \lim_{\substack{\omega\to\omega_e(\lambda),\\ \mathrm{Im}(\omega)>0}} \hat{\phi}(\omega,\lambda)[\omega-\omega_e(\lambda)] + \lim_{\substack{\omega\to\omega_e(\lambda),\\ \mathrm{Im}(\omega)<0}} \hat{\phi}(\omega,\lambda)[\omega-\omega_e(\lambda)]. \tag{B 7}$$

Thus $\omega_e(\lambda)$ is the dominant frequency, and (B 6) gives the associated eigenfunction excited by an initial condition corresponding to a single value of λ. For the example mentioned above of a Green's function of the linearized Euler equations, there are two singular frequencies $\omega_e(\lambda)=\omega_c(\lambda), \omega_c(r)$ (see § 4 of Heaton & Peake 2006) and the corresponding long-time behaviour is obtained by summing their contributions.

The energy $E(t)$ in our simplified system is given by $E(t)=|\phi|^2$. It is clear that, for any single value of λ, $E(t)=O(1)$ for all t. However, the transient mechanism described in § B.1, in which initial cancellations disappear at long times due to small differences in eigenfrequency, is realized by taking

$$\Phi(t)=\phi(t;\lambda+\epsilon)-\phi(t;\lambda), \tag{B 8}$$

where $\epsilon \ll 1$. From (B 6) it follows that at large times the energy of the particular solution (B 8) is

$$E(t) \sim \pi^2 \left|L(\lambda+\epsilon)\exp(-\mathrm{i}\omega_e'(\lambda)\epsilon t) - L(\lambda)\right|^2 \quad \text{for} \quad t \gg 1. \tag{B 9}$$

From (B 9) we get

$$E(t)=\begin{cases} O(\epsilon^2) & \text{for } t = O(1) \\ O(\epsilon^2 t^2) & \text{for } 1 \ll t \ll \epsilon^{-1} \\ O(1) & \text{for } t = O(\epsilon^{-1}), \end{cases} \tag{B 10}$$

and therefore this solution exhibits transient growth. The gain $G(t)$ is found by fixing t and varying ϵ to maximize the energy amplification. For $t \gg 1$, and fixed, it follows from (B 10) that

$$\frac{E(t)}{E(0)} = \begin{cases} o(t^2) & \text{for } t^{-1} \ll \epsilon \leqslant O(1) \\ O(t^2) & \text{for } \epsilon \leqslant t^{-1}. \end{cases} \tag{B 11}$$

Hence for $t \gg 1$ the gain is $O(t^2)$ large, and the overall maximum will be attained by a value of ϵ at least as small as t^{-1}. Note that for a value of λ in (B 8) such that $\omega_e'(\lambda)=0$, the results (B 10), (B 11) are altered slightly: the maximum energy amplification becomes $O(t)$, so this special case (if it occurs) is suboptimal and does not change the result that the maximum gain is quadratic in time.

B.3. *Non-neutral continuous spectra*

Now, the t^2 gain described above is the baseline result, for a flow or linear system with a neutrally stable continuous spectrum and no exponentially growing modes. If instead the flow is exponentially unstable, the gain of course will grow exponentially in time at the rate of the most unstable eigenfrequency. However, if there are no exponential instabilities but the continuous spectrum is not simply neutrally stable, then this will modify the t^2 result. More generally a flow's continuous spectrum can respond algebraically as $|\boldsymbol{u}| \sim t^{\sigma_{\max}}$, with $\sigma_{\max}$ not necessarily equal to 0.

On repeating the arguments of § B.1 with two frequencies close to one another on C_ω, and which exhibit algebraic growth with exponent $\sigma_{\max}$, we find that the initial kinetic energy $E(0)=O(\Delta\omega^2)$ as before, but that the energy is then elevated not to $O(1)$, but instead to $E(\Delta\omega^{-1})=O(\Delta\omega^{-2\sigma_{\max}})$. As before the two eigenvectors become fully uncorrelated, but also the two eigensolutions each have their amplitude altered

somewhat in the intervening time. Thus we obtain $G(t) \sim t^{2+2\sigma_{\max}}$ in this case. The arguments of § B.2 are modified by the presence of a stronger singularity in (B 5), which then alters the calculation. Ultimately the calculation gives $E(t) = O(t^{2\sigma_{\max}})$ for $t = O(\epsilon^{-1})$ in (B 10), implying again that the maximum gain $G(t) \sim t^{2+2\sigma_{\max}}$.

REFERENCES

Antkowiak, A. & Brancher, P. 2004 Transient growth for the Lamb–Oseen vortex. *Phys. Fluids* **16**, L1–L4.

Atassi, H. M., Ali, A. A., Atassi, O. V. & Vinogradov, I. V. 2004 Scattering of incident disturbances by an annular cascade in a swirling flow. *J. Fluid Mech.* **499**, 111–138.

Batchelor, G. K. 1964 Axial flow in trailing line vortices. *J. Fluid Mech.* **20**, 645–658.

Batchelor, G. K. & Gill, A. E. 1962 Analysis of the stability of axisymmetric jets. *J. Fluid Mech.* **14**, 529–551.

Ben-Dov, G., Levinski, V. & Cohen, J. 2004 Optimal disturbances in swirling flows. *AIAA J.* **42**, 1841–1848.

Bernoff, A. J. & Lingevitch, J. F. 1994 Rapid relaxation of an axisymmetric vortex. *Phys. Fluids* **6**, 3717–3723.

Boyd, J. P. 2001 *Chebyshev and Fourier Spectral Methods* 2nd edn. Dover.

Butler, K. M. & Farrell, B. F. 1992 Three-dimensional optimal perturbations in viscous shear flow. *Phys. Fluids* **4**, 1637–1650.

Chapman, S. J. 2002 Subcritical transition in channel flows. *J. Fluid Mech.* **451**, 35–97.

Cooper, A. J. & Peake, N. 2005 Upstream-radiated rotor–stator interaction noise in mean swirling flow. *J. Fluid Mech.* **523**, 219–250.

Cooper, A. J. & Peake, N. 2006 Transient growth and rotor–stator interaction noise in mean swirling duct flow. *J. Sound Vib.* **295**, 553–570.

Corbett, P. & Bottaro, A. 2000 Optimal perturbations for boundary layers subject to stream-wise pressure gradient. *Phys. Fluids* **12**, 120–130.

Duck, P. W. & Foster, M. R. 1980 The inviscid stability of a trailing line vortex. *Z. Angew. Math. Phys.* **31**, 524–532.

Fabre, D. & Jacquin, L. 2004 Viscous instabilities in trailing vortices at large swirl number. *J. Fluid Mech.* **500**, 239–262.

Fabre, D., Sipp, D. & Jacquin, L. 2006 Kelvin waves and the singular modes of the Lamb–Oseen vortex. *J. Fluid Mech.* **551**, 235–274.

Farrell, B. F. & Ioannou, P. J. 1993 Stochastic forcing of the linearized Navier–Stokes equations. *Phys. Fluids* A **5**, 2600–2609.

Gustavsson, L. H. 1991 Energy growth of three-dimensional disturbances in plane Poiseuille flow. *J. Fluid Mech.* **224**, 241–260.

Hanifi, A. & Henningson, D. S. 1998 The compressible inviscid algebraic instability for streamwise independent disturbances. *Phys. Fluids* **10**, 1784–1786.

Heaton, C. J. 2007 Centre modes in inviscid swirling flows and their application to the stability of the Batchelor vortex. *J. Fluid Mech.* **576**, 325–348.

Heaton, C. J. & Peake, N. 2006 Algebraic and exponential instability of inviscid swirling flow. *J. Fluid Mech.* **565**, 279–318.

Khorrami, M. R. 1991 On the viscous modes of instability of a trailing line vortex. *J. Fluid Mech.* **225**, 197–212.

Khorrami, M. R., Malik, M. R. & Ash, R. L. 1989 Application of spectral collocation techniques to the stability of swirling flows. *J. Comput. Phys.* **81**, 206–229.

Landahl, M. T. 1980 A note on an algebraic instability of inviscid parallel shear flows. *J. Fluid Mech.* **98**, 243–251.

Le Dizès, S. & Fabre, D. 2006 Large-Reynolds-number asymptotic analysis of viscous centre modes in vortices. *J. Fluid Mech.* (submitted).

Leibovich, S. 1978 The structure of vortex breakdown. *Annu. Rev. Fluid Mech.* **10**, 221–246.

Lessen, M. & Paillet, F. 1974 The stability of a trailing line vortex. Part 2. Viscous theory. *J. Fluid Mech.* **65**, 769–779.

Lessen, M., Singh, P. J. & Paillet, F. 1974 The stability of a trailing line vortex. Part 1. Inviscid theory. *J. Fluid Mech.* **63**, 753–763.

Lighthill, M. J. 1958 *An Introduction to Fourier Analysis and Generalised Functions*. Cambridge University Press.

Mayer, E. W. & Powell, K. G. 1992 Viscous and inviscid instabilities of a trailing vortex. *J. Fluid Mech.* **245**, 91–114.

Pradeep, D. S. & Hussain, F. 2006 Transient growth of perturbations in a vortex column. *J. Fluid Mech.* **550**, 251–288.

Schmid, P. J. & Henningson, D. S. 1994 Optimal energy density growth in Hagen–Poiseuille flow. *J. Fluid Mech.* **277**, 197–225.

Schmid, P. J. & Henningson, D. S. 2001 *Stability and Transition in Shear Flows*. Springer.

Schmid, P. J., Henningson, D. S., Khorrami, M. R. & Malik, M. R. 1993 A study of eigenvalue sensitivity for hydrodynamic stability operators. *Theor. Comp. Fluid Dyn.* **4**, 227–240.

Stewartson, K. & Brown, S. N. 1985 Near-neutral centre-modes as inviscid perturbations to a trailing line vortex. *J. Fluid Mech.* **156**, 387–399.

Thomson, W. 1887 (Lord Kelvin) Rectilineal motion of viscous fluid between two parallel planes. *Phil. Mag.* **24**, 188–196.

Trefethen, L. N., Trefethen, A. E., Reddy, S. C. & Driscoll, T. A. 1993 Hydrodynamic stability without eigenvalues. *Science* **261**, 578–584.